Title: F-actin regulates polarized secretion of pollen tube attractants in *Arabidopsis* synergid cell.

Short title: Roles of cytoskeletons in synergid cell.

Authors: Daichi Susaki[1], Rie Izumi[1], Takao Oi[2], Hidenori Takeuchi[3,4], Ji Min Shin[5] Naoya Sugi[1], Tetsu Kinoshita[1], Tetsuya Higashiyama[3,6,7], Tomokazu Kawashima[5] and Daisuke Maruyama[1]*.

Affiliations:

1. Kihara Institute for Biological Research, Yokohama City University, Maioka-cho 641-12, Totsuka-ku, Yokohama, Kanagawa, 244-0813, Japan.
2. Graduate school of Bioagricultural Sciences, Nagoya University, Furo-cho, Chikusa-ku, Nagoya, Aichi 464-8602, Japan.
3. Institute of Transformative Bio-Molecules (WPI-ITbM), Nagoya University, Furo-cho, Chikusa-ku, Nagoya, Aichi 464-8601, Japan.
4. Institute for Advanced Research, Nagoya University, Furo-cho, Chikusa-ku, Nagoya, Aichi 464-8601, Japan.
5. Department of Plant and Soil Sciences, University of Kentucky, 321 Plant Science Building, Lexington, KY 40546, USA.
6. Division of Biological Science, Graduate School of Science, Nagoya University, Furo-cho, Chikusa-ku, Nagoya, Aichi 464-8602, Japan.
7. Department of Biological Sciences, Graduate School of Science, The University of Tokyo, Hongo, Bunkyo-ku, Tokyo 113-0033, Japan.

* Author for correspondence: dmaru@yokohama-cu.ac.jp

Footnotes:

The author responsible for distribution of materials integral to the findings presented in this article in accordance with the policy described in the Instructions for Authors (https://academic.oup.com/plcell/pages/General-Instructions) is: Daisuke Maruyama (dmaru@yokohama-cu.ac.jp)."

Abstract

Pollen tube attraction is a key event of sexual reproduction in flowering plants. In the ovule, two synergid cells neighboring the egg cell control pollen tube arrival via the active secretion of attractant peptides such as AtLURE1 and XIUQIU from the filiform apparatus facing toward the micropyle. Distinctive cell polarity together with longitudinal F-actin and microtubules are hallmarks of the synergid cell in various species, though functions of these cellular structures are still unclear. In this study we used genetic and pharmacological approaches to elucidate the roles of cytoskeletal components in filiform apparatus formation and pollen tube guidance in *Arabidopsis thaliana*. Inhibition of microtubule formation reduced invaginations of the plasma membrane but did not abolish micropylar AtLURE1.2 accumulation. In contrast, the expression of a dominant-negative form of ACTIN8 induced disorganization of the filiform apparatus and loss of polar AtLURE1.2 distribution toward the filiform apparatus. Interestingly, after pollen tube reception, F-actin became unclear for a few hours in the persistent synergid cell, which may be involved in pausing and resuming pollen tube attraction during early polytubey block. Our data propose the central role of F-actin in the maintenance of cell polarity and function of male-female communication in the synergid cell.

(199 words)

53 ## Introduction

54 Sexual plant reproduction proceeds with multicellular haploid tissues termed
55 gametophytes. Most flowering plants, including *Arabidopsis thaliana,* produce a
56 *Polygonum*-type female gametophyte that contains seven cells: one egg cell, one central
57 cell, two synergid cells and three antipodal cells. On the other hand, pollen grains or
58 pollen tubes are the male gametophytes and contain fewer cells, with a tip-growing
59 pollen tube vegetate cell that contain two sperm cells. Sexual reproduction is
60 accomplished when the egg cell and central cell are fertilized by two sperm cells
61 delivered by the pollen tube. Although the synergid cell itself is not fertilized, it is
62 responsible for almost all communications between female and male gametophytes
63 prior to double fertilization. The synergid cell controls pollen tube attraction, pollen
64 tube reception, termination of pollen tube attraction, and fertilization recovery
65 (Dresselhaus et al., 2016).

66 In the past two decades, many synergid cell-specific genes have been identified
67 that are required for the communication between the female and male gametophytes. In
68 some species, various pollen tube attractants secreted from the synergid cell have been
69 identified: ZmEA1 in maize (Marton et al., 2005; Marton et al., 2012); LURE1 and
70 LURE2 in *Torenia* (Okuda et al., 2009); AtLURE1s, XIUQIUs, and TICKETs in *A.*
71 *thaliana* (Takeuchi and Higashiyama, 2012; Zhong et al., 2019; Meng et al., 2019).

72 Receptor-like kinases on the pollen tube tip, including PRK6, interact with AtLURE1
73 and control the directional growth of the pollen tube (Takeuchi and Higashiyama, 2016).
74 After arrival of the pollen tube, one of the two synergid cells receives the pollen tube
75 contents, including the two sperm cells. The receptive synergid regulates pollen tube
76 discharge via CrRLK1L-type receptor-like kinases such as FERONIA, ANJEA, and
77 HERCULES RECEPTOR KINASE 1 (HERK1) (Escobar-Restrepo et al., 2007;
78 Galindo-Trigo et al., 2020), a GPI-anchored protein LORELEI (Capron et al., 2008;
79 Tsukamoto et al., 2010), and a Mildew resistance locus o (MLO) family-related protein
80 NORTIA (Kessler et al., 2010). Genetic and biochemical approaches have begun to
81 uncover their cooperative mechanisms during pollen tube reception (Li et al., 2015; Ju
82 et al., 2021). Following pollen tube reception, ovules prevent the attraction of extra
83 pollen tubes, a process called polytubey block, reducing risk of egg cell fertilization by
84 more than one sperm cell known as polyspermy (Kasahara et al., 2012; Beale et al.,
85 2012; Maruyama and Higashiyama, 2016). In early ovular polytubey block, activated
86 just before or upon double fertilization, synergid cells produce nitric oxide (NO) in a
87 FERONIA dependent manner. The NO signal not only inactivates AtLURE1 peptides
88 via post-translational nitrosation, but also inhibits the AtLURE1 secretory system by an
89 unknown mechanism (Duan et al., 2020). In addition, the clearance of attractants may
90 be accelerated by fertilization-dependent secretion of aspartic endopeptidases from the
91 zygote (Yu et al., 2021). On the other hand, later stages of the polytubey block are

92 initiated a few hours after double fertilization by the inactivation of the non-receptive
93 persistent synergid. Representative features of the persistent synergid elimination are
94 nuclear degeneration and cell-to-cell fusion between the persistent synergid and the
95 endosperm (Völz et al., 2013; Maruyama et al., 2013; Maruyama et al., 2015; Pereira et
96 al., 2016). If ovules are not fertilized by the first pollen tube, they pause the
97 degeneration of the persistent synergid and resume the attraction of the next pollen tube
98 (Kasahara et al., 2012; Beale et al., 2012).

99 The synergid cell displays a highly polarized morphology, characterized by
100 concentration of the protoplasm at the micropylar side, facing toward the pollen tube
101 entry pathway in the ovule, and a large central vacuole occupies at the opposite chalazal
102 side (Mansfield et al., 1991). The micropylar end of the synergid cell has the filiform
103 apparatus, an active communication domain with complex plasma membrane
104 invaginations and thick cell walls, that presumably has pivotal roles in secreting plenty
105 of pollen tube attractant peptides and localizing pollen tube reception factors (Johnson
106 et al., 2019). Synergid cell shape formation and dynamic protein relocation or secretion
107 may be regulated by the cytoskeletons. Immunostaining studies have shown radial
108 microtubules spreading from the filiform apparatus in various species including *A.*
109 *thaliana* (Webb and Gunning, 1994). In contrast, filamentous actin (F-actin) is widely
110 distributed longitudinally along the micropyle-chalazal axis (Webb and Gunning, 1994).
111 However, the significance of the cytoskeletons in synergid cells remains unclear.

112 In this study, we aimed to investigate the functions of the cytoskeleton in *A.*
113 *thaliana* synergid cells. We used genetic and pharmacological approaches to induce
114 microtubule- and actin-depolymerization. Our results indicate that microtubule
115 destruction compromises the elongation of plasma membrane invaginations in the
116 filiform apparatus. On the other hand, disruption of F-actin caused severe
117 disorganization of synergid cell morphology, including phenotypic alterations such as
118 incomplete filiform apparatus formation and aberrant positions of the central vacuole.
119 Furthermore, F-actin destruction impaired the secretion of pollen tube attractant
120 peptides and caused female sterility. Interestingly, the longitudinal F-actin pattern
121 disappeared in the persistent synergid after pollen tube discharge, suggesting dynamic
122 regulation of F-actin during fertilization. Altogether, these findings elucidated flexibility
123 of the F-actin-mediated directional secretion system that maintains morphology and
124 function of the synergid cell.
125

126 **RESULTS**

127 **Morphology of filiform apparatus.**

128 Filiform apparatus was usually described as a finger-like structure from
129 observations of mature ovules by transmission electron microscopy (Jensen, 1965;
130 Diboll and Larson, 1966; Schulz and Jensen, 1968). To update our knowledge on the
131 filiform apparatus morphology, we conducted three-dimensional (3D) reconstruction of
132 mature *A. thaliana* ovule by focused ion beam-scanning electron microscopy
133 (FIB-SEM) (Oi et al., 2017). A 3D image reconstructed from the serial sections (713
134 sequential electron micrographs with 25 nm step size) showed a sponge-like porous
135 domain of cell walls at the micropylar end of the filiform apparatus, rather than the
136 finger-like pattern that are often used to depict filiform apparatus in 2D electron
137 micrographs (FA and Po in Figure 1A and 1B; Movie 1). According to the 3D model,
138 the surface area of plasma membrane in the filiform apparatus was 3.7-fold larger than
139 the presumed cell wall area excluding invaginations (72.3 μm^2 and 19.8 μm^2,
140 respectively).

141 Next, we generated a plasma membrane marker *pMYB98::3×mNG-SYP132*,
142 expressing Syntaxin of plant 132 (SYP132) tagged with tandem fusions of three
143 mNeonGreen from the synergid cell-specific *MYB98* promoter (Uemura et al., 2004;
144 Shaner et al., 2013; Kasahara et al., 2005) and analyzed complex structures of the

145 filiform apparatus in live synergid cells by confocal microscopy (Figure 1C; Movie 2).
146 Z-series confocal images showed that the porous structure exhibited strong fluorescent
147 signals due to the accumulations of vesicular- or folded-plasma membranes (Figure 1C,
148 Po). In contrast to the FIB-SEM data, we observed long protrusions of the tubular
149 plasma membrane from the porous area toward the inside of the cell (Figure 1C, Inv).
150 Among the eight synergid cells in the four ovules, we observed an average of 8.0±2.3
151 invaginations per cell with a length ranging from 1.8 to 11.5 μm (Figure 1C). The size
152 of the invagination was comparable between pairs of synergid cells from the same ovule
153 but varied among different ovules (Figure 1D). In addition, bulges were observed along
154 the invaginations in three ovules (Figure 1C, Bu).
155
156 **Morphology and dynamics of cytoskeletons in synergid cell.**
157 The formation of complex plant cell morphologies often requires F-actin and/or
158 microtubules (Eng and Sampathkumar, 2018). To investigate pattern of these
159 cytoskeletons in the live synergid cell, we generated a double marker line expressing an
160 F-actin binding Lifeact peptide tagged with mRUBY3 (Lifeact-mRUBY3) and
161 TUBULIN ALPHA 5 fused with Citrine (Citrine-TUA5) from the synergid cell-specific
162 *MYB98* promoter (Riedl et al., 2008; Shaner et al., 2013; Kasahara et al., 2005). In the
163 mature ovules, mRUBY3 signal of F-actin extended from the micropylar end, where the
164 filiform apparatus resides, and reached beyond synergid nuclei and large central

165 vacuoles to the chalazal end (Figure 2A, left panel). Citrine-labeled microtubules were
166 also longitudinally aligned around the filiform apparatus, forming a radially extended
167 cat-whisker pattern (Figure 2A, middle panel), where F-actin often associated or
168 co-localized with microtubules (Figure 2A, right panel).

169 In the egg cell and central cell, F-actin is generated at the cell periphery and
170 migrates toward the nucleus, supporting the rapid merger of female and male nuclei
171 (karyogamy) after gamete fusions (plasmogamy) (Kawashima et al., 2014; Ohnishi et
172 al., 2014; Ohnishi and Okamoto, 2015). To examine whether fertilization-incompetent
173 gametophytic cells (*i.e.,* synergid cells) have the similar nucleopetal F-actin dynamics,
174 we observed F-actin dynamics in the synergid cells of mature ovules
175 (*pMYB98::Lifeact-mNG*) by time-lapse imaging at 30 sec intervals. The movie showed
176 that actin cables actively moved longitudinally (Movie 3), and we further performed the
177 spatiotemporal image correlation spectroscopy analysis (Ashdown et al., 2015) to
178 evaluate directions of F-actin flow at four areas (two in the chalazal and one each in
179 peri-nuclear and micropylar regions). Radar plots indicated that the directions of F-actin
180 flow were mainly from chalazal to micropyle, except for the micropylar region (Figure
181 2B–2E and S2). Around the filiform apparatus, the F-actin flow was omnidirectional,
182 implying active rearrangements of F-actin. These results show that, unlike the
183 nucleopetal F-actin dynamics of the gametes, overall F-actin dynamics in the synergid
184 cell are toward the filiform apparatus.

185

186 **Genetic disruption of microtubule formation.**

187 To analyze the roles of microtubules in the synergid cell, we used PHS1ΔP, a
188 dominant mutant of PROPYZAMIDE-HYPERSENSITIVE 1 (PHS1). PHS1 is an α
189 -tubulin kinase consisting of a central tubulin kinase domain and a C-terminal
190 phosphatase domain (Fujita et al., 2013). PHS1ΔP lacks the C-terminal phosphatase
191 domain and shows high tubulin kinase activity, inducing microtubule depolymerization
192 via overproduction of polymerization-inefficient phosphorylated α-tubulins (Fujita et al.,
193 2013). We generated two transgenic lines homozygous for a transgene expressing the
194 *PHS1ΔP* from the *MYB98* promoter (*pMYB98::PHS1ΔP*) that were also homozygous
195 for two reporter genes visualizing synergid cell morphology: the
196 *pRPS5A::H2B-tdTomato* (*RHT*) and *pES2::3×mNG-SYP132* (ENS). *RHT* is a nuclear
197 marker expressing tdTomato-tagged HISTONE H2B from the ubiquitously active
198 *Ribosomal Protein Subunit 5A* promoter (Maruyama et al., 2013). As shown in Figure
199 S1, *ENS* is a plasma membrane marker expressing 3×mNeonGreen-SYP132 from the
200 embryo sac-specific *ES2* promoter (Yu et al., 2005; Pagnussat et al, 2007).

201 The mature ovules from the *pMYB98::PHS1ΔP;RHT;ENS* transgenic lines were
202 compared with those from the wild-type *RHT;ENS* line using confocal microscopy. In
203 wild-type *RHT;ENS*, 97.7% of the ovules contained the normal seven-celled female
204 gametophyte with two synergid cells, an egg cell, a central cell, and three antipodal cells

205 (Figure 3A, n = 386). On the other hand, in *pMYB98::PHS1ΔP;RHT;ENS*, only 9.3–
206 12.9% of the gametophytes showed normal cell structure (Figure 3B, Two synergids;
207 Figure 3F), and the remaining ovules exhibited varieties of aberrance. Specifically,
208 37.2–37.5% of the ovules contained a single synergid cell with either one or two nuclei
209 (Figure 3C, single synergid). Because the *MYB98* promoter becomes active prior to
210 cellularization of the eight-nucleate female gametophyte (Kasahara et al., 2005; Susaki
211 et al., 2021), these single synergid ovules were likely generated due to the inadequate
212 spindle and/or cell plate formation caused by PHS1ΔP-mediated microtubule
213 depolymerization (Figure 3C and 3F, SY-SY fusion). Consistently, we observed more
214 severe phenotypes in *pMYB98::PHS1ΔP;RHT;ENS*; including the disappearance of
215 mNeonGreen-labeled plasma membrane accumulation, a hallmark of the filiform
216 apparatus, in 49.5–53.6% of the ovules (Figure 3D and 3E, No FA). Occasionally, these
217 ovules contained no nuclei in the putative synergid region while the central cell had
218 multiple nuclei (Figure 3E, 9.5–10.3%). These phenotypes suggest that the absence of
219 the filiform apparatus may reflect the failure of synergid cell differentiation due to
220 incomplete cytokinesis between the two synergid cells and the central cell (Figure 3D–
221 3F, CC-SY fusion).

222 In the following experiments, we focused on the single-synergid ovules because
223 they were observed more frequently than the two-synergid ovules (Figure 3C and 3F).
224 Around the filiform apparatus, only ~10.0% of the single-synergid ovules produced

225 long plasma membrane invaginations (Figure 3C and 3G, greater than ~6 μm), which
226 was considerably fewer than that of normal synergid cells in the wild-type *RHT;ENS*
227 ovules (Figure 3A and 3G, 80.9%, n = 377). Next, we performed transmission electron
228 microscopy to analyze the cell walls at the filiform apparatus (Figure 3H–3K). In
229 wild-type *RHT;ENS*, the cell walls exhibited typical finger-like pattern consisting of an
230 electron dense central region surrounded by a translucent peripheral layer (Figure 3H
231 and 3I, 100%, n = 7). Similar finger-like cell walls were also observed in the
232 single-synergid ovules of *pMYB98::PHS1ΔP RHT;ENS* (Figure 3J and 3K, 80%, n = 5).
233 To investigate the expression and localization of the cytoskeletons and pollen tube
234 attractant, we introduced the microtubule, F-actin, and pollen tube attractant markers
235 into the wild-type *RHT* and *pMYB98::PHS1ΔP;RHT* lines (Figure 3L–3Q). The
236 single-synergid ovules carrying *pMYB98::PHS1ΔP* displayed no fibers, visualized using
237 the *pMYB98::Citrine-TUA5* microtubule marker, confirming the significant effect of
238 PHS1ΔP expression microtubule depolymerization (Figure 3L and 3M). Normal
239 longitudinal F-actin *(pMYB98::Lifeact-mNeonGreen)* was observed in the
240 single-synergid ovules of the *pMYB98::PHS1ΔP* line (Figure 3N and 3O). Finally, the
241 pollen tube attractant marker, *pAtLURE1.2::AtLURE1.2-Citrine*, showed a comparable
242 Citrine focus at the filiform apparatus in both wild-type and *pMYB98::PHS1ΔP* lines,
243 indicating of normal polarized secretion in these ovules (Figure 3P and 3Q). Altogether,
244 these results suggest that whisker-like microtubules facilitate the growth of plasma

245 membrane invaginations but have a limited effect on the formation of the basal structure
246 of the filiform apparatus and cell polarity.

247 To investigate pollen tube attraction and fertility, pistils from the wild-type
248 *RHT;ENS* and *pMYB98::PHS1ΔP;RHT;ENS* lines were pollinated with the
249 non-transgenic Col-0 pollen (Figure 4). At one-day-after pollination (1 DAP), pollen
250 tubes were visualized by CongoRed staining. In the wild-type *RHT;ENS* pistils, 97.5%
251 of the ovules received pollen tubes and displayed nuclear proliferation in the endosperm,
252 showing successful pollen tube attraction and fertilization (Figure 4A, n = 360). Similar
253 fertilization phenotypes were also observed in 49.7% of the ovules from
254 *pMYB98::PHS1ΔP;RHT;ENS* plants (Figure 4B, n = 338), which corresponded to the
255 total frequency of the single-synergid and two-synergid ovules (Figure 3B, 3C, 3F). The
256 remaining 50.3% did not proliferate the endosperm nuclei (Figure 4C–4E and 4G),
257 implying fertilization abnormalities in these ovules, which also showed no plasma
258 membrane accumulation at the filiform apparatus (Figure 3D–F). In the
259 *pMYB98::PHS1ΔP;RHT;ENS* plants, normal seed development was observed in ~70%
260 at 10 DAP (Figure 4H–4J), which were comparable to the ovules receiving a pollen tube
261 at 1 DAP (Figure 4F). Thus, the subset of the PHS1ΔP-expressing ovules might show
262 fertilization delay soon after pollen tube reception (Figure 4C and 4F, 22,2%) and would
263 be gradually fertilized by 8 DAP. Taken together, PHS1ΔP-mediated microtubule
264 depolymerization and the loss of long invaginations at the filiform apparatus would not

265 abolish pollen tube attraction and reception by the synergid cell.

266

267 **Expression of a dominant-negative actin in the synergid cell caused severe defect in**

268 **pollen tube attraction.**

269 To examine the roles of F-actin in synergid cell, we generated transgenic plants

270 expressing wild-type ACTIN8 (*WT-ACTIN*) or the dominant-negative form of ACTIN8

271 (*DN-ACTIN*) from the *MYB98* promoter. Homozygous plants were not recovered in four

272 independent *pMYB98::DN-ACTIN* lines, implying reduced fertility in the female

273 gametophyte. To further investigate that, we compared 8 DAP seeds in pistils from

274 Col-0 wild-type plants and *pMYB98::DN-ACTIN* hemizygous mutants pollinated with

275 Col-0 wild-type pollen (Figure 5A–5C). Wild-type pistils contained almost full sets of

276 seeds (Figure 5A and 5C). However, approximately half of the ovules remained

277 undeveloped in the *pMYB98::DN-ACTIN* line (Figure 5B and 5C). Next, we analyzed

278 the hygromycin resistance in these F_1 siblings. Hygromycin resistance in the

279 *pMYB98::WT-ACTIN* hemizygous line was 52.7%, suggesting normal inheritance in the

280 *pMYB98::WT-ACTIN* plants from the female gametophyte (Figure 5D). Nevertheless,

281 hygromycin resistance in the four *pMYB98::DN-ACTIN* hemizygous lines ranged from

282 2.8 to 9.5% (Figure 5D). When wild-type Col-0 pistils were pollinated with pollen from

283 the *pMYB98::WT-ACTIN* or *pMYB98::DN-ACTIN* hemizygous plants, no reproductive

284 abnormalities, such as reduced seed set or decreased hygromycin resistance, were

285 observed in the F_1 siblings (Figure 5C and 5E). Taken together, we concluded that the
286 *pMYB98::DN-ACTIN* caused sterility exclusively in the female gametophyte.

287 To further investigate the cause of female sterility, we first examined pollen
288 tube attraction. Pistils from wild-type and *pMYB98::DN-ACTIN* plants were pollinated
289 with wild-type Col-0 pollen, and the pollen tube growth pattern was analyzed at 1 DAP
290 using CongoRed staining. In wild-type pistils, 96.2% of the ovules received the pollen
291 tube, indicative of successful pollen tube attraction (Figure 5F and 5H, n = 227),
292 whereas pollen tube attraction was observed only in 51.3% of the ovules from the
293 *pMYB98::DN-ACTIN* line (Figure 5G and 5H, n = 463). Therefore,
294 *pMYB98::DN-ACTIN* may reduce ovule fertility through a pollen tube guidance defect.

295

296 **Loss of F-actin in the synergid cell impairs secretion of pollen tube attractant**
297 **peptides.**

298 The pollen tube attraction defect observed in *pMYB98::DN-ACTIN* may be
299 explained by a decrease in the secretion of pollen tube attractant peptides from the
300 synergid cell. To assess this hypothesis, we compared the immunostaining pattern of
301 AtLURE1.2 in mature ovules from non-transgenic Col-0, *myb98* homozygous, and
302 *pMYB98::DN-ACTIN* hemizygous plants (Figure S3). AtLURE1.2 signals were detected
303 on the surface of the micropyle and/or funiculus in ~90% of the ovules from
304 non-transgenic Col-0 plants (Figure S3A; n = 206). The AtLURE1.2 signal was below

305 the detection level in the *myb98* homozygous mutant, as reported previously (Figure
306 S3B; n = 231; Takeuchi and Higashiyama, 2012). In the *pMYB98::DN-ACTIN*
307 hemizygous plant, AtLURE1.2 signals were only observed in ~40% of the ovules
308 (Figure S3C; n = 260), indicating a reduction of AtLURE1.2 secretion in the *DN-ACTIN*
309 expressing ovules. To further examine pollen tube attractants in the synergid cells, we
310 used a translational fusion reporter of *AtLURE1.2* and *Citrine*
311 (*pAtLURE1.2::AtLURE1.2-Citrine*). Consistent with the previous report, the fluorescent
312 signal of AtLURE1.2-Citrine was specifically observed in the synergid cell with the
313 strongest signal detected at the filiform apparatus (97.0%, n = 339; Figure 6A, 6B and
314 6G; Takeuchi and Higashiyama, 2012). In the *pMYB98::DN-ACTIN* hemizygous plants
315 that were homozygous for the *pAtLURE1.2::AtLURE1.2-Citrine*, Citrine signal was
316 detected in 92.9% of ovules (n = 432; Figure 6C–6D), suggesting that DN-ACTIN had
317 little or no effect on cell differentiation and gene expression in the synergid cell.
318 However, a normal AtLURE1.2-Citrine secretion pattern was observed only in 46.3% of
319 ovules (WT; Figure 6C, 6D and 6G). In the remaining ovules that were expected to
320 carry *pMYB98::DN-ACTIN*, AtLURE1.2-Citrine did not accumulate at the filiform
321 apparatus but rather was uniformly distributed in the cytoplasm (*pMYB98::DN-ACTIN*;
322 Figure 6E and 6F). Abnormalities were also observed in the central vacuole. Wild-type
323 ovules presented single large central vacuole at the chalazal side (Figure 6B and 6D),
324 whereas ovules from *pMYB98::DN-ACTIN* hemizygous line often contained multiple

325 small vacuoles located in the middle or micropylar side of the synergid cell (Figure 6F).
326 In agreement, similar results were obtained with the pollen tube attractant marker,
327 *XIUQIU4-Citrine* (Figure S4). These data indicate the aberrant secretion of AtLURE1.2
328 and XIUQIU4 in the DN-ACTIN expressing synergid cells.

329 We next analyzed the ultrastructure of normal and abnormal ovules segregated
330 from *pMYB98::DN-ACTIN* hemizygous plants that were homozygous for
331 *pAtLURE1.2::AtLURE1.2-Citrine* (Figure 6H–6K). Although normal ovules with a
332 strong Citrine signal at the filiform apparatus showed finger-like cell walls (Figure 6H
333 and 6I; n = 7), abnormal ovules accumulated electron-dense cell wall materials with
334 chaotic pattern (Figure 6J and 6K; n = 5). To examine other morphological aspects of
335 the abnormal synergid cell, marker genes for the plasma membrane and cytoskeletons
336 were introduced into *DN-ACTIN* expressing lines. In the *pMYB98::DN-ACTIN*
337 hemizygous plants that were homozygous for *pES2::3×mNG-SYP132* (*ENS*), 48.6% of
338 the ovules exhibited a normal filiform apparatus pattern, characterized by the
339 accumulation and invagination of mNeonGreen-labeled plasma membrane at the
340 filiform apparatus (Figure 6L; n = 436). The remaining ovules (51.4%) did not have
341 mNeonGreen focus at the micropylar end, and vesicles of various sizes were detected
342 inside of the synergid cell (Figure 6M), suggesting disorganization of the filiform
343 apparatus in the *pMYB98::DN-ACTIN* line. In the *pMYB98::DN-ACTIN* hemizygous
344 plants that were homozygous for *pMYB98::Lifeact-mNeonGreen*, 49.3% of the ovules

345 produced longitudinally aligned F-actin as wild-type ovules observed in Figure 2
346 (Figure 6M; n = 319), while the remaining ovules showed fragmented F-actin and
347 destruction of the actin cable alignment (Figure 6M). On the other hand, typical
348 whisker-like microtubule extensions at the filiform apparatus did not change between
349 normal and abnormal ovules in the *pMYB98::DN-ACTIN* hemizygous plants that were
350 homozygous for the *pMYB98::Citrine-TUA5* (Figure 6P and 6Q; n = 212). The
351 Citrine-TUA5 pattern indicates independence of F-actin formation and microtubule
352 formation in the synergid cell.

353 The analyses of the *pMYB98::DN-ACTIN* transgenic lines revealed important
354 roles of F-actin in pollen tube attraction. However, this genetic approach could not
355 clarify whether the pollen tube attraction defect was induced by the loss of the filiform
356 apparatus or inhibition of attractant peptide secretion. Thus, we examined changes in
357 synergid cell morphology within a few hours after actin polymerization inhibition by
358 Latrunculin A (LatA) treatment. First, we confirmed that half-an-hour treatment with
359 100 μM LatA diminished F-actin in synergid cell from the *pMYB98::Lifeact-mNG* line
360 (Figure 7A and 7B). Interestingly, *pMYB98::Citrine-TUA5* synergid cell displayed
361 normal whisker-like microtubule extensions after 100 μM LatA treatment (Figure 7C
362 and 7D), indicating independent regulation of F-actin and microtubules in the synergid
363 cell. In addition, plasma membrane accumulation and invaginations at the filiform
364 apparatus visualized with *pES2::3×mNG-SYP132* were not altered even 4h after 100

365 μM LatA treatment (Figure 7E and 7F). Nevertheless, drastic alterations were observed
366 in the *pAtLURE1.2::AtLURE1.2-Citrine* line; which showed a Citrine signal focused at
367 the filiform apparatus in control DMSO-treated ovules that disappeared 4h after 100 μM
368 LatA treatment, which also induced the appearance of smaller vacuoles (Figure 7G and
369 7H). The LatA-mediated AtLURE1.2-Citrine signal alterations resembled the
370 phenotypes induced by the genetic F-actin destruction in the *pMYB98::DN-ACTIN* lines
371 (Figure 6E and 6F), suggesting that F-actin destruction quickly stalls
372 AtLURE1.2-Citrine secretion in synergid cell even in the presence of a functional
373 filiform apparatus. A similar analysis was performed by treating
374 *pAtLURE1.2::AtLURE1.2-Citrine*, *pES2::3×mNG-SYP132*, *pMYB98::Lifeact-mNG*,
375 and *pMYB98::Citrine-TUA5* lines with the microtubule polymerization inhibitor,
376 Oryzalin (Figure S5). However, an altered fluorescent pattern was observed only with
377 the *pMYB98::Citrine-TUA5* microtubule marker (Figure S5C and S5D). Taken together,
378 these results suggest that F-actin regulates the polarized secretion of pollen tube
379 attractant peptides at the filiform apparatus.
380

381 **Temporal disappearance of longitudinal F-actin in persistent synergid cell after**
382 **pollen tube discharge.**

383 Cumulative evidence supporting F-actin-mediated pollen tube attraction
384 prompted us to investigate F-actin pattern in the persistent synergid during fertilization

385 because it may be involved in the cessation of pollen tube attraction observed after
386 successful double fertilization (Kasahara et al., 2012; Beale et al., 2012). Pistils from
387 *pMYB98::Lifeact-mNG* were pollinated with pollens from a sperm cell-specific nuclear
388 marker *pHTR10::HTR10-mRFP1* (Ingouff et al., 2007), and ovules were analyzed by
389 spinning disk confocal microscopy at 6 h-after-pollination (6 HAP) (Figure 8A–8I). In
390 the unfertilized ovules, normal longitudinal F-actin pattern was observed in both intact
391 synergid cells on different focal planes (Figure 8A, 8E, and 8I). By contrast, different
392 F-actin pattern was observed in two synergid cells after pollen tube reception.
393 According to the sperm nuclei-derived mRFP1 signals, fertilization states of these
394 ovules were classified into three categories: before plasmogamy, before karyogamy, and
395 after karyogamy. Ovules before plasmogamy contained sperm cells closely apposed
396 each other between the egg cell and central cell (Figure 8B and 8F). In the ovules before
397 karyogamy, each separated sperm nucleus was observed in the egg cell and central cell
398 (Figure 8C and 8G). In ovules after karyogamy, the sperm-derived mRFP1 signal was
399 dispersed in the zygote nucleus or primary endosperm nucleus by chromatin
400 decondensation in ovules after karyogamy (Figure 8D and 8H). Throughout these
401 fertilization stages, actin cables were unclear in the receptive synergid and the
402 fluorescent proteins leaked into and marked the boundary of the egg cell and central cell
403 (Figure 8B–8D). In addition, we often observed mNeonGreen foci around the chalazal
404 end of the receptive synergid, which may correspond to the “actin corona” visualized by

405 Rhodamine-phalloidin staining in *Nicotiana tabacum* ovules (Russell, 1993; Huang and
406 Russell, 1994). When the pistils from *pMYB98::Lifeact-mNG* were fertilized by the
407 tagRFP-expressing pollen tubes (*pLAT52::tagRFP*), we found moderate colocalization
408 of cytosolic tagRFP with the actin corona-like structure (Figure S6).

409 In contrast to the receptive synergid, the persistent synergid did not show actin
410 corona-like structures and the actin cables disappeared before plasmogamy (Figure 8F
411 and 8I; n = 31). The percentage of ovules containing visible actin cables slightly
412 increased at the stage before karyogamy (Figure 8G and 8I; 34%, n = 38), and finally
413 reached 58% after karyogamy (Figure 8H and 8I; n = 85). To examine whether actin
414 cable recovery depended on plasmogamy, we used *gcs1*, a T-DNA insertion allele of
415 *GENERATIVE CELL SPECIFIC 1/HAPLESS2* that produces plasmogamy-defective
416 sperm cells (Mori et al., 2006; von Besser et al., 2006). Pistils from
417 *pMYB98::Lifeact-mNG* were pollinated with the pollens from *gcs1* heterozygous plants
418 carrying *pHTR10::HTR10-mRFP1*, and the F-actin pattern in the persistent synergid
419 was analyzed in ovules containing unfused sperm cells at 6, 9, and 14 HAP (Figure 8J
420 and 8K). At 14 HAP, clear actin cables were observed in the ovules more frequently
421 than at earlier HAP time points (Figure 8K), indicating the fertilization-independent
422 nature of actin cable recovery. To elucidate the regeneration process of actin cables, we
423 next performed a time-lapse imaging. Pistils from *pMYB98::Lifeact-mNG* were
424 pollinated with the pollens from *gcs1/+;pHTR10::HTR10-mRFP1*, and 6 HAP ovules

425 cultured in a liquid medium were observed every 15 min by spinning disk confocal
426 microscopy. In fertilized ovules, persistent synergids were absorbed within a few hours
427 and the F-actin pattern was no longer visible due to the rapid dilution of
428 Lifeact-mNeonGreen (Movie 4). In contrast, ovules containing unfused sperm cells
429 maintained the mNeonGreen signal in the persistent synergid through the 12 hours of
430 time-lapse observation (Figure 8L; Movie 5). In these unfertilized ovules, few actin
431 cables emerged ~3h after observation and the actin cables gradually increased the
432 number. These results indicate that pollen tube discharge induces temporal actin
433 depolymerization and cell-autonomous regeneration of actin cables in the persistent
434 synergid.
435

436 **DISCUSSION**

437 The synergid cell has been extensively studied as the key regulator of the initial
438 communication between male and female gametophytes during fertilization in flowering
439 plants. In this study, genetic and pharmacological approaches revealed different roles of
440 microtubules and F-actin in the morphology and functions of synergid cell. Although
441 partial colocalization of microtubules and actin cables was observed in the synergid cell,
442 F-actin disruption did not affect microtubule pattern and *vice versa* (Figure 2; Figure 3;
443 Figure 6; Figure 7; Figure S5). These observations imply independent functions of the

444 two cytoskeletal components in the synergid cell. Indeed, different phenotypes were
445 observed after disruption of microtubule or F-actin formation. Inhibition of microtubule
446 formation by PHS1ΔP expression led to shorter plasma membrane invaginations at the
447 filiform apparatus, whereas the ovules accomplished pollen tube attraction and
448 fertilization normally (Figure 3; Figure 4). On the other hand, F-actin deformation
449 compromised the polarity of synergid cell organelles and impaired the secretion of
450 pollen tube attractants from the filiform apparatus (Figure 6; Figure 7). Therefore, we
451 propose that longitudinal actin cables play a central role in the formation and
452 maintenance of cell polarity, while microtubules have subsidiary roles in filiform
453 apparatus formation.

454 Our FIB-SEM and confocal microscopy analyses revealed a detailed sponge-like
455 filiform apparatus structure consisting of plasma membranes and cell walls (Figure 1).
456 The porous cell wall pattern was severely impaired by the expression of DN-ACTIN
457 (Figure 6), suggesting that the proper cell wall pattern at the filiform apparatus requires
458 coordination of actin-mediated protein secretion and cell wall formation. The loss of
459 plasma membrane accumulation was also observed in the PHS1ΔP expressing ovules
460 probably due to the stochastic fusions of two synergid cells and central cell (Figure 3).
461 Interestingly, a subset of this type of ovules may accomplish pollen tube attraction,
462 double fertilization, and seed formation (Figure 4). Although details of the
463 synergid-central cell fused cell with multifunction are still unclear, our data indicate the

464 capability of pollen tube attraction and reception in the absence of plasma membrane
465 invaginations at the filiform apparatus. If the filiform apparatus is dispensable from the
466 synergid cell, why this complex structure is conserved among flowering plants? The
467 role of complexity at the filiform apparatus may not be confined to only surface
468 expansion of the protein secretion area. Perhaps, the porous cell walls may serve as a
469 genuine sponge for the temporary storage of signaling molecules to ensure efficient
470 reproduction. For example, this putative signal storage might support accurate pollen
471 tube attraction by buffering fluctuations of protein secretion. Alternatively, it may
472 modulate pollen tube behavior through the release of a large amount of signaling
473 molecules when the growing pollen tube tip pushes the filiform apparatus before pollen
474 tube discharge (Higashiyama et al., 1998; Leshem et al., 2013; Ngo et al., 2014).

475 Not only pollen tube attractant peptides, but also various pollen tube reception
476 factors such as FERONIA, ANJEA, HERK1, LORELEI, and NORTIA are localized at
477 the plasma membrane of the filiform apparatus (Escobar-Restrepo et al., 2007;
478 Galindo-Trigo et al., 2020; Capron et al., 2008; Tsukamoto et al., 2010; Kessler et al.,
479 2010). NORTIA is relocated from a Golgi-associated compartment to the filiform
480 apparatus during pollen tube reception, implying cargo-dependent spatiotemporal
481 control of polarized protein secretion in the synergid cell. Polarized protein secretion
482 has been extensively studied in tip-growing model cells including the pollen tube, root
483 hair cell, protonema in mosses, and filamentous fungi (Stephan, 2017; Bibeau et al.,

484 2018). In these cells, F-actin is often concentrated beneath the tip region forming the
485 actin fringe, which facilitates the accumulation of secretory vesicles and subsequent
486 control of polarized secretions crucial for tip-growth (Stephan, 2017). Although F-actin
487 concentration was not obvious around the filiform apparatus, their active rearrangement
488 may be involved in polarized protein secretion as actin fringes in tip-growing cells.

489 The movement toward the filiform apparatus was another feature of F-actin
490 dynamics observed in the synergid cell. This is considerably different from actin
491 dynamics in the egg cell and central cell, where actin cables emerge from the cell
492 periphery and move toward the nucleus (Kawashima et al., 2014; Ohnishi et al., 2014;
493 Ohnishi and Okamoto, 2015). The nucleopetal movement in the female gametes is
494 regulated by an Arp2/3-independent WAVE/SCAR actin nucleation pathway activated
495 by ROP small GTPase and is important for the migration of sperm nuclei after
496 plasmogamy (Ali et al., 2020). Although the female gametophyte cells are originated
497 from the same cell lineage, their functions, morphology, and gene expression are quite
498 different at maturity. Therefore, the synergid cell may present its actin dynamics
499 controlled by a different set of actin modifiers including ROP, Arp2/3, WAVE/SCAR,
500 Formins, and other actin-binding proteins. The F-actin regulator, SCAR2 controls
501 F-actin meshwork movement in the central cell and possibly in the egg cell (Ali et al.,
502 2020). In our previous study, the synergid cells in *myb98* mutant, lacking extensive
503 invaginations characteristic of the filiform apparatus, have partially egg cell-like gene

504 expression and nuclear position. In the *myb98* synergid cell, slight upregulation in
505 *SCAR2* expression (Susaki et al., 2021) supports the hypothesis of cell-specific
506 regulation of actin in the female gametophyte cells.

507 In our observation, F-actin pattern in the synergid cell changes drastically during
508 fertilization. After pollen tube discharge, fine actin cables disappeared in the ruptured
509 receptive synergid and the synergid-derived Lifeact-mNeonGreen signal appeared as an
510 actin corona (Figure 8). Actin corona was discovered by a Rhodamine-phalloidin
511 staining to observe actin cables around discharged sperm cells prior to double
512 fertilization in *Nicotiana tabacum* (Russell, 1993; Huang and Russell, 1994). Due to its
513 characteristic spatiotemporal pattern, actin corona was speculated to transport the
514 released sperm cells to the area where double fertilization takes place. However,
515 live-imaging of double fertilization in direct delivery of sperm cells within a few
516 seconds, implying actin-independent sperm cell delivery mechanism in *A. thaliana*
517 (Hamamura et al., 2011). In this study, we found the actin corona-like signal
518 accumulation of the Lifeact-mNeonGreen exhibited moderate colocalization with
519 cytosolic tagRFP released from the pollen tube (Figure S6). Actin corona may be an
520 ephemeral cytosol accumulation irrelevant to sperm cell migration.

521 The persistent synergid displayed temporal disappearance of actin cables after
522 pollen tube discharge, which may pause secretion of pollen tube attractant peptides and
523 be involved in the mechanisms controlling polytubey block (Maruyama and

524 Higashiyama, 2016). Polytubey block is completed by the degeneration of the persistent
525 synergid triggered by double fertilization. The degeneration processes include a
526 cell-fusion between the persistent synergid and endosperm (Maruyama et al., 2015) and
527 degeneration of the persistent synergid nucleus, which is mediated by the EIN3 and
528 EIL1 transcription factors (Völz et al., 2013; Li et al., 2022; Heydlauff et al., 2022) and
529 FIS-class polycomb repressive complex (Maruyama et al., 2013; Maruyama et al.,
530 2015). Compared to these late degeneration processes, the disappearance of actin cables
531 may be an earlier and fertilization-independent alteration that temporarily inactivates
532 persistent synergid functions (Figure 8F, 8I, 8J–K). Recent reports have demonstrated
533 several early polytubey block pathways that diminish the attractant signals around the
534 micropyle. Specifically, FERONIA-dependent NO production accompanying with a
535 deposition of de-esterified pectin inactivates AtLURE1 peptides via post-translational
536 nitrosation upon pollen tube arrival (Duan et al., 2020). Active AtLURE1 peptides are
537 further reduced by ECS1 and ECS2, which are egg cell-specific aspartic endopeptidases
538 secreted immediately after plasmogamy (Yu et al., 2021). Together with these attractant
539 peptides elimination systems, inhibition of protein secretion in the persistent synergid
540 should play a key role in the early polytubey block. Termination of AtLURE1 secretion
541 and intracellular accumulation of AtLURE1 in the synergid cell are also induced by
542 elevation of NO signaling during pollen tube arrival (Duan et al., 2020). Although the
543 precise mechanism is still unknown, the NO-mediated termination of AtLURE1

544 secretion may be controlled by the temporal destruction of actin cables. Further studies
545 using inhibitors and mutants affecting NO production and F-actin formation are
546 required to confirm this hypothesis.

547 Interestingly, the persistent synergid displayed actin cables regeneration, which
548 was more evident in unfertilized ovules after reception of the plasmogamy-defective
549 *gcs1* mutant pollen tube (Figure 8L). When the first pollen tube fails to fertilize the
550 female gametes, the ovules stop the degeneration of the persistent synergid and begin to
551 attract a second pollen tube within ~5h (Kasahara et al., 2012; Duan et al., 2020; Zhong
552 et al., 2022). The time window between the arrival of the first and second pollen tubes
553 coincides with the period of actin cable disappearance in the persistent synergid,
554 suggesting that actin cables dynamics of destruction-reconstruction function as a
555 courtship-pause timer allowing the persistent synergid to attract the second pollen tube.
556 Occasionally, polytubey causes polyspermy, which might provide the offspring
557 agronomically useful traits inherited from three parents (Nakel et al., 2017;
558 Grossniklaus, 2017; Mao et al, 2020). To increase the efficiency of such polyspermy
559 breeding, cell biology of persistent synergid reactivation would become important in the
560 future. Our discovery of the actin cable regeneration could be the first step to
561 understanding molecular mechanism of the persistent synergid reactivation.
562

563 ## Methods

564 **Plant materials and growth conditions**

565 Columbia-0 (Col-0) was used as the wild-type strain. The *gcs1* (SALK_135694)
566 heterozygous mutant that was also homozygous for the *pHTR10::HTR10-mRFP* has been
567 described previously (Kasahara et al, 2012). Seeds were surface sterilized with
568 sterilization solution (2% PLANT PRESERVATIVE MIXTURE ™, 0.1% Tween 20) and
569 incubated at 4ºC for several days and sown on Murashige and Skoog (MS) medium
570 containing 1% sucrose and appropriate antibiotics. Approximately 10 days after
571 germination, plants were transferred to soil. Plants were grown at 22°C under continuous
572 light or standard long day conditions.

573

574 **Plasmids and transgenic plants**

575 The *pRPS5A::H2B-tdTomato* plasmid was kindly provided by D. Kurihara
576 (Nagoya Univ.) (Maruyama et al., 2013). pDM286, a pGWB501 destination vector
577 (Nakagawa et al., 2007) containing the *MYB98* promoter, has been reported previously
578 (Maruyama et al., 2015). The *pAGL80::tagRFP-TUA5*, pDM230 (a binary vector
579 carrying the *pLAT52::tagRFP*) and the pSNA128 (a pGWB501 destination vector
580 containing 1,062 bp upstream of the coding region of the *ES2* (At1g26795) (Pagnussat
581 et al, 2007; Hwang et al., 2019)) were gifts from Shuh-ichi Nishikawa (Niigata Univ.).
582 The primers used for plasmid constructions are listed in Table S1.

583 The *PHS1ΔP*, a mutant gene of C-terminus-truncated
584 PROPYZAMIDE-HYPERSENSITIVE 1 (85–700 a.a.) (Fujita et al., 2013), was
585 amplified from *Arabidopsis* seedling cDNA by a PCR using primers

586 ‘PHS1dP_F+SalI-TOPO’ and ‘PHS1dP_R+AscI-stop’, and introduced into
587 pENTR/D-TOPO vector (Invitrogen) to generate the HTv1243. An LR recombination
588 between the pDM286 and HTv1243 produced pDM580, a binary vector containing the
589 *pMYB98::PHS1ΔP*.

590 The HTv1313 and HTv1316, two pollen tube attractant reporter plasmids were
591 cloned as follows. The coding sequence of yellow fluorescent protein Citrine was
592 introduced into pPZP211 vector by replacing mRuby2 of pPZP211Ru (Takeuchi and
593 Higashiyama, 2016), resulting in pPZP211Cit. The entire genomic sequence of
594 *AtLURE1.2* including the protein-coding and upstream promoter sequences was
595 amplified from *Arabidopsis* genomic DNA by a PCR using primers
596 ‘AtLURE1.2_F+SalIGA’ and ‘AtLURE1.2_-stopR+AscIGA’, and introduced into the
597 SalI/AscI site of the pPZP211Cit to produce the HTv1313, a binary vector harboring the
598 *pAtLURE1.2::AtLURE1.2-Citrine*. Similarly, entire genomic sequence of the
599 CRP810_2.3/XIUIQIU4/TIC3 was amplified by a PCR using primers
600 ‘810_2.3_F+SalIGA’ and ‘810_2.3_-stopR+AscIGA’, and introduced into the SalI/AscI
601 site of the pPZP211Cit to produce the HTv1316, a binary vector harboring the
602 *XIUQIU4::XIUQIU4-Citrine*.

603 To generate the synergid cell-specific F-actin reporter genes, a DNA fragment of
604 *mNeonGreen*- or *mRUBY3*-tagged *Lifeact* was amplified by PCR using primers ‘pENTR
605 LifeActFP_F’ and ‘FP_R’ and cloned into pENTR/D-TOPO to produce pOR099 or
606 pOR102. An LR recombination between the pDM286 and pOR099 produced pDM522, a
607 binary vector containing the *pMYB98::Lifeact-mNG*, and an LR recombination between
608 the pDM286 and pOR102 produced pDM523, a binary vector containing the
609 *pMYB98::Lifeact-mRUBY3*.

610 To generate the synergid cell-specific microtubule reporter gene, a DNA fragment
611 of *mTFP1* was amplified by PCR using primers 'pENTR_CFP_F' and 'FP_PstI_R' and
612 cloned into pENTR/D-TOPO. Then, *TUA5* sequence in the *pAGL80::tagRFP-TUA5* was
613 introduced into *Nco*I/*Pst*I site of the *mTFP1*-containing entry vector to produce pOR103.
614 The *Citrine* coding sequence was amplified from the HTv1313 by a PCR using primers
615 'pENTR_cacc_XFP_F' and 'FP_PstI_R', and substituted with *mTFP1* in the pOR103 by
616 *Nco*I/*Pst*I digestion and subsequent ligation to generate pOR177. An LR recombination
617 between the pDM286 and pOR177 produced pDM680, a binary vector containing the
618 *pMYB98::Citrine-TUA5*.

619 Plasma membrane markers were constructed as follows. The pOR084, an entry
620 clone containing *mRUBY2-SYP132*, was constructed using NEBuilder HiFi DNA
621 Assembly Cloning Kit (New England Biolabs, MA, USA) by multi-DNA fragment
622 assembly between (i) *mRUBY2*-containing pENTR/D-TOPO (Thermo Fisher Scientific,
623 MA, USA) plasmid backbone amplified by a primer set 'FP_SpeI_F' and 'FP_EcoRI_R'
624 and (ii) *SYP132* (At5g08080) cDNA sequence amplified by a primer set
625 'SYP132_EcoRI_F' and 'SYP132_SpeI_R'. pENTR/D-TOPO plasmid backbone with
626 the *SYP132* was amplified from the pOR084 by a PCR using primers 'GFP_1-18_R' and
627 'XFP_C-term_F'. Resulting linearized plasmid DNA was mixed with three mNeonGreen
628 DNA fragments independently amplified by the following three primer sets, 'GFP F' and
629 'Linker1_XFP_R', 'Linker1_XFP_F' and 'Linker2_XFP_R', or 'Linker2_XFP_F' and
630 'FP_R', and multi-DNA fragment assembly by the NEBuilder HiFi DNA Assembly
631 Cloning Kit was performed to produce pOR129. An LR recombination of the pSNA128
632 and pOR129 generated *pES2::3×mNG-SYP132*. An LR recombination of the pDM286
633 and pOR129 generated *pMYB98::3×mNG-SYP132*. Two plasmids containing wild-type

634 *ACTIN8* (At1g49240) or dominant negative mutant of *ACTIN8* (Kato et al., 2010)
635 downstream of the *MYB98* promoter, were constructed by LR recombination between
636 the pDM286 and the entry clones carrying wild-type or dominant negative *ACTIN8* that
637 described in previously (Kawashima et al., 2014).

638 Agrobacterium-mediated plant transformation was performed by the floral
639 dipping method using Agrobacterium strain GV3101 (Clough and Bent, 1998).
640 Transformants were selected on MS medium containing 50 μg/mL hygromycin B or 50
641 μg/mL kanamycin.

642

643 **Analysis of mature ovules.**

644 Pistils were harvested one to two days after emasculation and the carpel walls
645 were removed on a glass slide. Then, the pistils were split into half and mounted on 5%
646 sucrose or an ovule culture medium containing Nitsch basal salt mixture (Duchefa) and
647 5% trehalose dihydrate (Wako Fujifilm) (Gooh et al., 2015). In pharmacological assay,
648 Latrunculin A or Oryzalin were dissolved in DMSO to make 2.5 mM stock solutions
649 and stored at -20ºC. These stock solutions were thawed and diluted 250 times by the
650 ovule culture media before use (final concentration, 100 μM). Mature ovules were
651 incubated in these inhibitor-containing media or 0.4% DMSO (negative control), and
652 confocal images were obtained by Leica SP8 TCS (Leica, Wetzlar, Germany). For
653 time-lapse imaging, ovules were dissected from pistils in a droplet of ovule culture
654 medium containing Nitsch basal salt mixture (Duchefa) and 5% trehalose dihydrate

655 (Wako Fujifilm) (Gooh et al., 2015), and transferred to a glass bottom dish (D141410;
656 Matsunami Glass IND., LTD., Japan). XY positions of the ovules were recorded by
657 bright field observation, and time-lapse confocal images were captured using IX73
658 inverted microscope (Olympus, Tokyo, Japan) equipped with a spinning disk confocal
659 scanning unit (CSU-W1; Yokogawa, Tokyo, Japan) and an sCMOS camera (Zyla 4.2;
660 Andor, Belfast, Northern Ireland).
661

662 **Analysis of seed phenotypes**

663 Siliques at eight day-after-pollination were attached on a glass slide by
664 double-sided tape and the upper side of the carpel walls were removed by an ophthalmic
665 knife. The samples were imaged by a dissecting microscope Leica E4 W (Leica, Wetzlar,
666 Germany). To investigate frequency of normal seeds, we harvested fully matured
667 siliques and counted normal seeds and undeveloped seeds under dissecting microscope.
668

669 **Histochemistry**

670 CongoRed staining was performed as previously described by Kasahara et al., (2005)
671 with slight modification. Dissected pistils at 1 day-after-pollination were treated with
672 0.4% CongoRed Solution for 1 min on a glass slide and washed several times with 5%
673 sucrose. Immuno-Staining of AtLURE1.2 was performed as reported previously
674 (Takeuchi and Higashiyama, 2012). These samples were observed by an upright

675 microscope (Axio Imager. M1; Zeiss, Jera, Germany) using filter sets for DsRed or GFP.
676 Epi-fluorescent images of those pistils were captured by the IX73 inverted microscope
677 (Olympus, Tokyo, Japan).
678
679 **FIB-SEM**
680 FIB-SEM sample blocks were prepared as follows. Wild-type Col-0 ovules
681 were fixed overnight in a fixation solution (4% paraformaldehyde, 2% glutaraldehyde,
682 0.05 M cacodylate buffer), then washed three times with 0.05 M cacodylate buffer. The
683 samples were subjected to postfixation with osmium tetroxide in 0.05 M cacodylate
684 buffer at 4ºC for 1h and washed five times with distilled water. After incubation with
685 1% thiocarbohydrazide for 20 min and five rounds of wash with distilled water, the
686 ovules were treated with 2% aqueous osmium tetroxide at room temperature for 1h and
687 washed three times with distilled water. The samples were stained overnight with 1%
688 aqueous uranyl acetate at 4ºC, then treated with 0.03M lead aspartate at 60ºC for 30
689 min. The tissue was then dehydrated with increasing ethanol concentrations (50%, 70%,
690 90%, 100%), transferred into propylene oxide, infiltrated, and embedded in Quetol 651.
691 Specimens were analyzed by FIB-SEM as described previously (Oi et al., 2017). Briefly,
692 the surfaces of the embedded ovules were exposed using a diamond knife on an
693 ultramicrotome (EM UC6; Leica, Wetzlar, Germany), and the resin blocks were
694 trimmed to a cuboid and were attached on the standard specimen stage for FIB-SEM as

695 the exposed ovules faced the SEM column. The specimens were coated with a thin layer
696 using a carbon coater (CADE-E, Meiwafosis, Tokyo, Japan) to prevent electron
697 charging. The serial electron micrographs were obtained with a FIB-SEM (MI-4000L,
698 Hitachi, Tokyo, Japan). The FIB was operated with following conditions: accelerating
699 voltage, 30 kV; beam current for milling to prepare or to cut, 1.6 or 1.2 nA,
700 respectively; cutting interval (z-step), 25 nm. The SEM was operated with following
701 conditions: accelerating voltage, 1.0 kV; working distance, 2 mm; image size, 2000
702 ×2000 pixels; color depth, 8-bit (256 grey scales); pixel size, 25 nm per pixel.
703 Secondary and backscattered electrons were detected by the detector in the SEM
704 column (U+EsB). The images of serial sections were processed using the software 'Fiji'
705 (http://fiji.sc/Fiji) (Schindelin et al., 2012); grey scale was inverted, brightness and
706 contrast were adjusted, the images were aligned using the 'Register Virtual Stack Slices'
707 (Translation－Translation -no deformation) tool, and then the region of the filiform
708 apparatus was cropped (image size, 400 ×400 pixels). The outline of cell walls of two
709 synergid cells in all 2D images were traced manually using the software 'PaintTool SAI'
710 (ver. 1, Systemax, Japan). The inside region of the two synergid cells were binarized to
711 detect the filiform apparatus and to reconstruct it into the 3D model using the software
712 'Image-Pro Premier 3D' (ver. 9.3, Media Cybernetics, USA); the surface rendering
713 model was reconstructed with subsampling (64M voxel) and smoothing (low-pass filter
714 [3:3:3]), and then their surface area were calculated with the function '3D Measure'.

715

716 **Transmission electron microscopy**

717 Emasculated pistils from the transgenic plant homozygous for the *pMYB98::PHS1ΔP*,
718 *pRPS5A::H2B-tdTomato*, and *pES2::3×mNG-SYP132*, were dissected on glass slides
719 and analyzed by an upright microscope (Axio Imager. M1; Zeiss, Jera, Germany) to
720 select the ovules containing single synergid cell. Similarly, normal and abnormal ovules
721 were selected from the *pAtLURE1.2::AtLURE1.2-Citrine transgenic plant hemizygous*
722 *for the pMYB98::DN-ACTIN*. The ovule selection procedure was skipped when we
723 prepared wild-type controls of the cytoskeleton-disrupted transgenic plants. The ovules
724 were fixed in a solution containing 4% paraformaldehyde, 2% glutaraldehyde, and 50
725 mM sodium cacodylate at pH7.4 for several days at 4°C. The samples were washed in
726 buffer and post-fixed for 6 h in 2% aqueous osmium tetroxide at 4°C. The specimens
727 were then dehydrated in a graded ethanol series, transferred into propylene oxide,
728 infiltrated, and embedded in Quetol 651. Series of thin-sections (80 nm) were stained
729 with 2% aqueous uranyl acetate and lead citrate, and examined at 80 kV under a JEOL
730 JEM 1400 Plus electron microscope (JEOL Ltd.). Digital images were taken with a
731 CCD camera (VELETA; Olympus Soft Imaging Solutions).

732

733 **Analysis of F-actin flow**

734 Time-lapse images of F-actin dynamics in synergid cell expressing

735 *pMYB98::Lifeact-mNG* were captured by spinning disk confocal microscopy with 30 sec
736 intervals (total 21 frames; 600 sec) and multiple z-planes (total 9 planes, 1 μm intervals).
737 The image was deconvoluted using the constrained iterated deconvolution function of
738 CellSens Dimension Desktop 3.2 (Olympus). Background noise was removed using the
739 subtract background function in Fiji (Schindelin et al., 2012). Three z-planes including
740 the peri-nuclear areas of the time-lapse images were projected and then used for
741 analysis of F-actin flow in the synergid cell. To analyze the F-actin flow, flow velocity
742 vectors (v_x,v_y) were obtained from spatio-temporal image correlation spectroscopy
743 analysis using MATLAB (MATLAB Inc.) scripts (Ashdown et al., 2015) with parameter
744 settings: pixelSize 0.259, timeframe 30, tauLimit 4, filtering FourierWhole,
745 MoveAverage 21, ROIsize 16, ROIshift 4, TOIsize 3, TOIshift 1 as described in the
746 manual (Ashdown et al., 2015). After the flow velocity vectors were acquired from each
747 analysis area, all angles of the flow velocity vectors from the entire analyzed frames
748 were calculated and normalized as probability using a custom MATLAB script to get
749 direction distribution of the F-actin flow.
750

751 **Conflict of interest**

752 The authors declare that the research was conducted in the absence of any commercial or
753 financial relationships that could be construed as a potential conflict of interest.
754

Author contributions

D.M. and T. Ka. conceived this project; D.S. obtained confocal images in Figure S1, 2 and S2; T.O. conducted FIB-SEM analysis and image processing in Figure 1 and Movie 1; J.M.S., T. Ka., and D.S. analyzed F-actin dynamics in Figure 2, S2 and Movie 3. R.I. and D.M. analyzed fertility of DN-ACTIN expressing lines; R.I and H.T. contributed immunostaining in Figure S2; N.S. analyzed the invagination length in Figure1; D.M. obtained other data and directed this project; D.M. and D.S. wrote the manuscript and all authors contributed to edit the manuscript.

Acknowledgements

FIB-SEM observation was supported by Nagoya University microstructural characterization platform as a program of "Nanotechnology Platform" of the Ministry of Education, Culture, Sports, Science and Technology (MEXT), Japan, and we especially thank S. Arai and S. Enomoto (Nagoya Univ.) for technical support. We acknowledge B. Raj Thapa (Univ. of Kentucky) for supporting on the F-actin movement quantification, M. Tsukatani for assistance in image analysis, H. Ikeda for assistance in preparing materials, D. Kurihara (Nagoya Univ.), S. Nishikawa (Niigata Univ.) and T. Nakagawa (Shimane Univ.) for providing plasmids. We would like to thank Editage (www.editage.com) for English language editing.

Funding

This work was supported by TOYOAKI Scholarship Foundation, Japan Society for the Promotion of Science (JSPS) KAKENHI [Grant Numbers: 17H05846, 19H04869, 20H03280, 20H05778 and

20H05781 to D.M.; 19K16172 and 22K15145 to D.S.; 18K14729 and 20K15817 to H.T.], by the Grant for academic research from Yokohama City University (to D.M.), by the grant for 2016–2022 Research Development Fund of Yokohama City University (to D.M.), and by National Science Foundation Grant IOS-1928836 (to T.Ka.).

781 ## References

782 Ashdown, G., Pandžić, E., Cope, A., Wiseman, P., and Owen, D. (2015) Cortical Actin
783 Flow in T Cells Quantified by Spatio-temporal Image Correlation Spectroscopy of
784 Structured Illumination Microscopy Data. JoVE: 53749.
785 Beale KM, Leydon AR, Johnson MA. (2012) Gamete fusion is required to block
786 multiple pollen tubes from entering an *Arabidopsis* ovule. Curr Biol 22: 1090–1094
787 Capron A, Gourgues M, Neiva LS, Faure JE, Berger F, Pagnussat G, Krishnan A,
788 Alvarez-Mejia C, Vielle-Calzada JP, Lee YR, et al. (2008) Maternal control of
789 male-gamete delivery in Arabidopsis involves a putative GPI-anchored protein
790 encoded by the LORELEI gene. Plant Cell 20: 3038–3049
791 Clough SJ, Bent AF. (1998) Floral dip: a simplified method for
792 Agrobacterium-mediated transformation of *Arabidopsis thaliana*. Plant J 16: 735–
793 743
794 Diboll AG, Larson DA. (1966) An electron microscopic study of the mature
795 megagametophyte in *Zea mays*. Am J Bot 53: 391–402
796 Dresselhaus T, Sprunck S, Wessel GM. (2016) Fertilization Mechanisms in Flowering
797 Plants. Curr Biol 26: R125–139
798 Duan Q, Liu MJ, Kita D, Jordan SS, Yeh FJ, Yvon R, Carpenter H, Federico AN,
799 Garcia-Valencia LE, Eyles SJ, et al., (2020) FERONIA controls pectin- and nitric
800 oxide-mediated male-female interaction. Nature 579: 561–566
801 Eng RC, Sampathkumar A. (2018) Getting into shape: the mechanics behind plant
802 morphogenesis. Curr Opin Plant Biol 46: 25–31
803 Escobar-Restrepo JM, Huck N, Kessler S, Gagliardini V, Gheyselinck J, Yang WC,
804 Grossniklaus U. (2007) The FERONIA receptor-like kinase mediates male-female
805 interactions during pollen tube reception. Science 317: 656–660
806 Fujita S, Pytela J, Hotta T, Kato T, Hamada T, Akamatsu R, Ishida Y, Kutsuna N,
807 Hasezawa S, Nomura Y et al. (2013) An atypical tubulin kinase mediates
808 stress-induced microtubule depolymerization in *Arabidopsis*. Curr Biol 23: 1969–
809 1978
810 Galindo-Trigo S, Blanco-Tourinan N, DeFalco TA, Wells ES, Gray JE, Zipfel C, Smith
811 LM. (2020) CrRLK1L receptor-like kinases HERK1 and ANJEA are female
812 determinants of pollen tube reception. EMBO Rep 21: e48466
813 Gooh K, Ueda M, Aruga K, Park J, Arata H, Higashiyama T, Kurihara D. (2015)
814 Live-cell imaging and optical manipulation of Arabidopsis early embryogenesis. Dev
815 Cell 34: 242–251
816 Grossniklaus U. (2017) Polyspermy produces tri-parental seeds in maize. Curr Biol 27:
817 R1300–R1302
818 Hamamura Y, Saito C, Awai C, Kurihara D, Miyawaki A, Nakagawa T, Kanaoka MM,
819 Sasaki N, Nakano A, Berger F. et al. (2011) Live-cell imaging reveals the dynamics

820 of two sperm cells during double fertilization in *Arabidopsis thaliana*. Curr Biol 21:
821 497–502
822 Heydlauff J, Serbes IE, Vo D, Mao Y, Gieseking S, Nakel T, Harten T, Völz R,
823 Hoffmann A, Groß-Hardt R. (2022) Dual and opposing roles of EIN3 reveal a
824 generation conflict during seed growth. Mol plant. 15: 363–371.
825 Higashiyama T, Kuroiwa H, Kawano S, Kuroiwa T. (1998) Guidance in vitro of the
826 pollen tube to the naked embryo sac of *Torenia fournieri*. Plant Cell 10: 2019–2031
827 Huang B-Q, Russell SD. (1994) Fertilization in *Nicotiana tabacum*: cytoskeletal
828 modifications in the embryo sac during synergid degeneration. Planta 194: 200–214
829 Hwang D, Wada S, Takahashi A, Urawa H, Kamei Y, Nishikawa SI. (2019)
830 Development of a Heat-Inducible Gene Expression System Using Female
831 Gametophytes of *Arabidopsis thaliana*. Plant Cell Physiol 60: 2564–2572
832 Ingouff M, Hamamura Y, Gourgues M, Higashiyama T, Berger F. (2007) Distinct
833 dynamics of HISTONE3 variants between the two fertilization products in plants.
834 Curr Biol 17: 1032–1037
835 Iwano M, Ngo QA, Entani T, Shiba H, Nagai T, Miyawaki A, Isogai A, Grossniklaus U,
836 Takayama S. (2012) Cytoplasmic Ca2+ changes dynamically during the interaction
837 of the pollen tube with synergid cells. Development 139: 4202–4209
838 Jensen WA. (1965) The ultrastructure and histochemistry of the synergids of cotton. Am
839 J Bot 52: 238–256
840 Johnson MA, Harper JF, Palanivelu R. (2019) A Fruitful Journey: Pollen Tube
841 Navigation from Germination to Fertilization. Annu Rev Plant Biol 70: 809–837
842 Ju Y, Yuan J, Jones DS, Zhang W, Staiger CJ, Kessler SA. (2021) Polarized NORTIA
843 accumulation in response to pollen tube arrival at synergids promotes fertilization.
844 Dev Cell 56: 2938–2951 e6
845 Kawashima T, Maruyama D, Shagirov M, Li J, Hamamura Y, Yelagandula R, Toyama Y,
846 Berger F. (2014) Dynamic F-actin movement is essential for fertilization in
847 *Arabidopsis thaliana*. Elife 3: e04501
848 Kasahara RD, Portereiko MF, Sandaklie-Nikolova L, Rabiger DS, Drews GN. (2005)
849 MYB98 is required for pollen tube guidance and synergid cell differentiation in
850 *Arabidopsis*. Plant Cell 17: 2981–2992.
851 Kasahara RD, Maruyama D, Hamamura Y, Sakakibara T, Twell, D, Higashiyama, T.
852 (2012) Fertilization recovery after defective sperm cell release in *Arabidopsis*. Curr.
853 Biol. 22: 1084–1089.
854 Kato T, Morita MT, Tasaka M. (2010) Defects in dynamics and functions of actin
855 filament in Arabidopsis caused by the dominant-negative actin *fiz1*-induced
856 fragmentation of actin filament. Plant Cell Physiol 51: 333–338
857 Kessler SA, Shimosato-Asano H, Keinath NF, Wuest SE, Ingram G, Panstruga R,
858 Grossniklaus U. (2010) Conserved molecular components for pollen tube reception
859 and fungal invasion. Science 330: 968–971

860 Li C, Yeh FL, Cheung AY, Duan Q, Kita D, Liu MC, Maman J, Luu EJ, Wu BW, Gates
861 L et al. (2015) Glycosylphosphatidylinositol-anchored proteins as chaperones and
862 co-receptors for FERONIA receptor kinase signaling in *Arabidopsis*. Elife 4: e06587
863 Li W, Li Q, Lyu M, Wang Z, Song Z, Zhong S, Gu H, Dong J, Dresselhaus T, Zhong S
864 et al. (2022) Lack of ethylene does not affect reproductive success and synergid cell
865 death in Arabidopsis. Mol Plant 15: 354–362
866 Mansfield SG, Briarty LG, Erni S. (1991) Early embryogenesis in Arabidopsis thaliana.
867 I. The mature embryo sac. Can J Bot 69: 447–460
868 Mao Y, Gabel A, Nakel T, Viehöver P, Baum T, Tekleyohans DG, Vo D, Grosse I,
869 Groß-Hardt R. (2020) Selective egg cell polyspermy bypasses the triploid block.
870 Elife 9: e52976
871 Marton ML, Cordts S, Broadhvest J, Dresselhaus T. (2005) Micropylar pollen tube
872 guidance by egg apparatus 1 of maize. Science 307: 573–576
873 Marton ML, Fastner A, Uebler S, Dresselhaus T. (2012) Overcoming hybridization
874 barriers by the secretion of the maize pollen tube attractant ZmEA1 from Arabidopsis
875 ovules. Curr Biol 22: 1194–1198
876 Maruyama D, Hamamura Y, Takeuchi H, Susaki D, Nishimaki M, Kurihara D, Kasahara
877 RD, Higashiyama T. (2013) Independent control by each female gamete prevents the
878 attraction of multiple pollen tubes. Dev Cell 25: 317–323
879 Maruyama D, Völz R, Takeuchi H, Mori T, Igawa T, Kurihara D, Kawashima T, Ueda
880 M, Ito M, Umeda M et al. (2015) Rapid Elimination of the Persistent Synergid
881 through a Cell Fusion Mechanism. Cell 161: 907–918
882 Maruyama D, Higashiyama T. (2016) The end of temptation: the elimination of
883 persistent synergid cell identity. Curr Opin in Plant Biol 34: 122–126
884 Meng J-G, Zhang M-X, Yang, W-C, Li H-J. (2019) TICKET attracts pollen tubes and
885 mediates reproductive isolation between relative species in Brassicaceae. Sci China
886 Life Sci 62: 1413–1419
887 Mori T, Kuroiwa H, Higashiyama T, Kuroiwa T. (2006) GENERATIVE CELL
888 SPECIFIC 1 is essential for angiosperm fertilization. Nat Cell Biol 8: 64–71
889 Nakagawa T, Suzuki T, Murata S, Nakamura S, Hino T, Maeo K, Tabata R, Kawai T,
890 Tanaka K, Niwa Y et al. (2007) Improved Gateway binary vectors: high-performance
891 vectors for creation of fusion constructs in transgenic analysis of plants. Biosci
892 Biotechnol Biochem 71: 2095–2100
893 Nakel T, Tekleyohans DG, Mao Y, Fuchert G, Vo D, Groß-Hardt R. (2017) Triparental
894 plants provide direct evidence for polyspermy induced polyploidy. Nat commun. 8:
895 1–8
896 Ngo QA, Vogler H, Lituiev DS, Nestorova A, Grossniklaus U. (2014) A calcium dialog
897 mediated by the FERONIA signal transduction pathway controls plant sperm
898 delivery. Dev Cell 29: 491–500
899 Ohnishi Y, Hoshino R, Okamoto T. (2014) Dynamics of Male and Female Chromatin

900 during Karyogamy in Rice Zygotes Plant Physiol 165: 1533–1543
901 Ohnishi Y, Okamoto T. (2015) Karyogamy in rice zygotes: Actin filament-dependent
902 migration of sperm nucleus, chromatin dynamics, and de novo gene expression
903 Plant Signal & Behav 10: e989021
904 Oi T, Enomoto S, Nakao T, Arai S, Yamane K, Taniguchi M. (2017) Three-dimensional
905 intracellular structure of a whole rice mesophyll cell observed with FIB-SEM. Ann
906 Bot 120: 21–28
907 Okuda S, Tsutsui H, Shiina K, Sprunck S, Takeuchi H, Yui R, Kasahara RD, Hamamura
908 Y, Mizukami A, Susaki D, et al. (2009) Defensin-like polypeptide LUREs are pollen
909 tube attractants secreted from synergid cells. Nature 458: 357–361
910 Pagnussat GC, Yu HJ, Sundaresan V. (2007) Cell-fate switch of synergid to egg cell in
911 Arabidopsis *eostre* mutant embryo sacs arises from misexpression of the BEL1-like
912 homeodomain gene BLH1. Plant Cell 19: 3578–3592
913 Pereira AM, Nobre MS, Pinto SC, Lopes AL, Costa ML, Masiero S, Coimbra S. (2016)
914 "Love Is Strong, and You're so Sweet": JAGGER Is Essential for Persistent Synergid
915 Degeneration and Polytubey Block in Arabidopsis thaliana. Mol Plant 9: 601–614
916 Leshem Y, Johnson C, Sundaresan V. (2013) Pollen tube entry into the synergid cell of
917 Arabidopsis is observed at a site distinct from the filiform apparatus. Plant
918 reproduction 26: 93–99.
919 Riedl J, Crevenna AH, Kessenbrock K, Yu JH, Neukirchen D, Bista M, Bradke F, Jenne
920 D, Holak TA, Werb Z et al. (2008) Lifeact: a versatile marker to visualize F-actin.
921 Nat. Methods 5: 605–607.
922 Russell SD. (1993) The egg cell: development and role in fertilization and early
923 embryogenesis. Plant Cell 5: 1349–1359
924 Schindelin J, Arganda-Carreras I, Frise E, Kaynig V, Longair M, Pietzsch T, Preibisch S,
925 Rueden C, Saalfeld S, Schmid B et al. (2012) Fiji: an open-source platform for
926 biological-image analysis. Nature methods 9: 676-82.
927 Schulz R, Jensen, WA. (1968) Capsella embryogenesis: the synergids before and after
928 fertilization. Am J Bot 55: 541–552
929 Shaner NC, Lambert GG, Chammas A, Ni Y, Cranfill PJ, Baird MA, Sell BR, Allen JR,
930 Day RN, Israelsson M et al. (2013) A bright monomeric green fluorescent protein
931 derived from *Branchiostoma lanceolatum*. Nat. Methods 10: 407–409
932 Stephan OOH. (2017) Actin fringes of polar cell growth. J Exp Bot 68: 3303–3320
933 Susaki D, Suzuki T, Maruyama D, Ueda M, Higashiyama T, Kurihara D. (2021)
934 Dynamics of the cell fate specifications during female gametophyte development in
935 *Arabidopsis*. PLoS Biol 19: e3001123
936 Takeuchi H, Higashiyama T. (2012) A species-specific cluster of defensin-like genes
937 encodes diffusible pollen tube attractants in Arabidopsis. PLoS Biol 10: e1001449
938 Takeuchi H, Higashiyama T. (2016) Tip-localized receptors control pollen tube growth
939 and LURE sensing in Arabidopsis. Nature 531: 245–248

940 Tsukamoto T, Qin Y, Huang Y, Dunatunga D, Palanivelu R. (2010) A role for LORELEI,
941 a putative glycosylphosphatidylinositol-anchored protein, in Arabidopsis thaliana
942 double fertilization and early seed development. Plant J 62: 571–588
943 Uemura T, Ueda T, Ohniwa RL, Nakano A, Takeyasu K, Sato MH. (2004) Systematic
944 analysis of SNARE molecules in Arabidopsis: dissection of the post-Golgi network
945 in plant cells. Cell Struc. Funct. 29: 49–65.
946 Völz R, Heydlauff J, Ripper D, von Lyncker L, Groß-Hardt R. (2013) Ethylene
947 signaling is required for synergid degeneration and the establishment of a pollen tube
948 block. Dev Cell 25: 310–316
949 von Besser K, Frank AC, Johnson MA, Preuss D. (2006) Arabidopsis HAP2 (GCS1) is
950 a sperm-specific gene required for pollen tube guidance and fertilization
951 Development 133: 4761–4769
952 Webb MC, Gunning BES. (1994) Embryo sac development in *Arabidopsis thaliana* II.
953 The cytoskeleton during megagametogenesis. Sex. Plant Reprod. 7: 153–163
954 Yu HJ, Hogan P, Sundaresan V. Analysis of the female gametophyte transcriptome of
955 Arabidopsis by comparative expression profiling. Plant physiology. (2005) 139:
956 1853–1869.
957 Yu X, Zhang X, Zhao P, Peng X, Chen H, Bleckmann A, Bazhenova A, Shi C,
958 Dresselhaus T, Sun MX. (2021) Fertilized egg cells secrete endopeptidases to avoid
959 polytubey. Nature 592: 433–437
960 Zhong S, Liu M, Wang Z, Huang Q, Hou S, Xu YC, Ge Z, Song Z, Huang J, Qiu X et al.
961 (2019) Cysteine-rich peptides promote interspecific genetic isolation in Arabidopsis.
962 Science 364: eaau9564
963
964 Zhong S, Li L, Wang Z, Ge Z, Li Q, Bleckmann A, Wang J, Song Z, Shi Y, Liu T et al.
965 (2022) RALF peptide signaling controls the polytubey block in Arabidopsis. Science
966 375: 290-296.
967
968

969 **Figures and Figure legends**

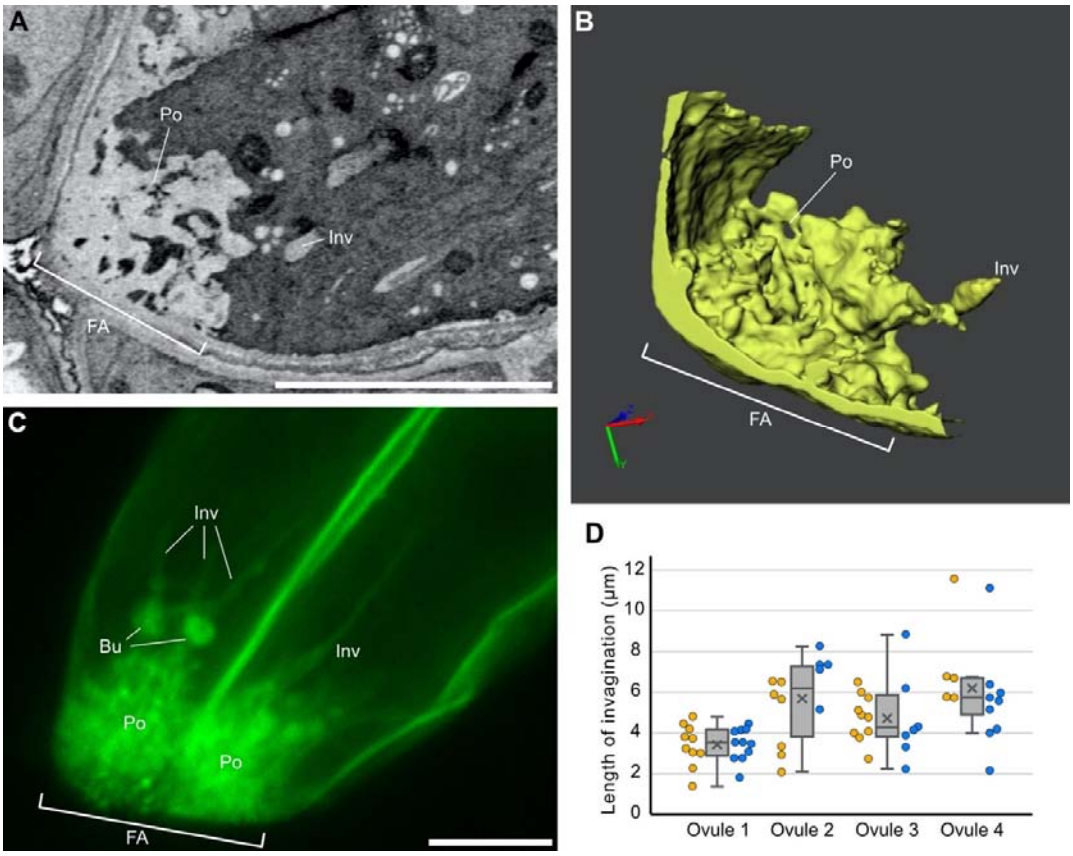

970

971

972 **Figure 1** Morphology of filiform apparatus in *Arabidopsis thaliana*. **A, B,** Filiform
973 apparatus analyzed by FIB-SEM (See also Movie 1). A single plane selected from the
974 serial section (A). 3D reconstruction image of the synergid cell wall (B). **C,** Plasma
975 membrane pattern visualized by *pMYB98::3×mNG-SYP132*. A maximum intensity
976 projection from the selected Z-serial sequences in Movie 2 is shown. **D,** Length of
977 plasma membrane invaginations at the filiform apparatus in the
978 *pMYB98::3×mNG-SYP132* plants. Box-and-whisker plots show median (center line),
979 mean (cross mark), upper and lower quartiles (box), maximum and minimum (whiskers),
980 and left and right points corresponding the data from each synergid cell (orange and
981 blue solid circles). Abbreviations: FA, filiform apparatus; Po, porous structure; Inv,
982 invagination; Bu, bulge. Scale bars: 5 μm in (A) and **(**C).

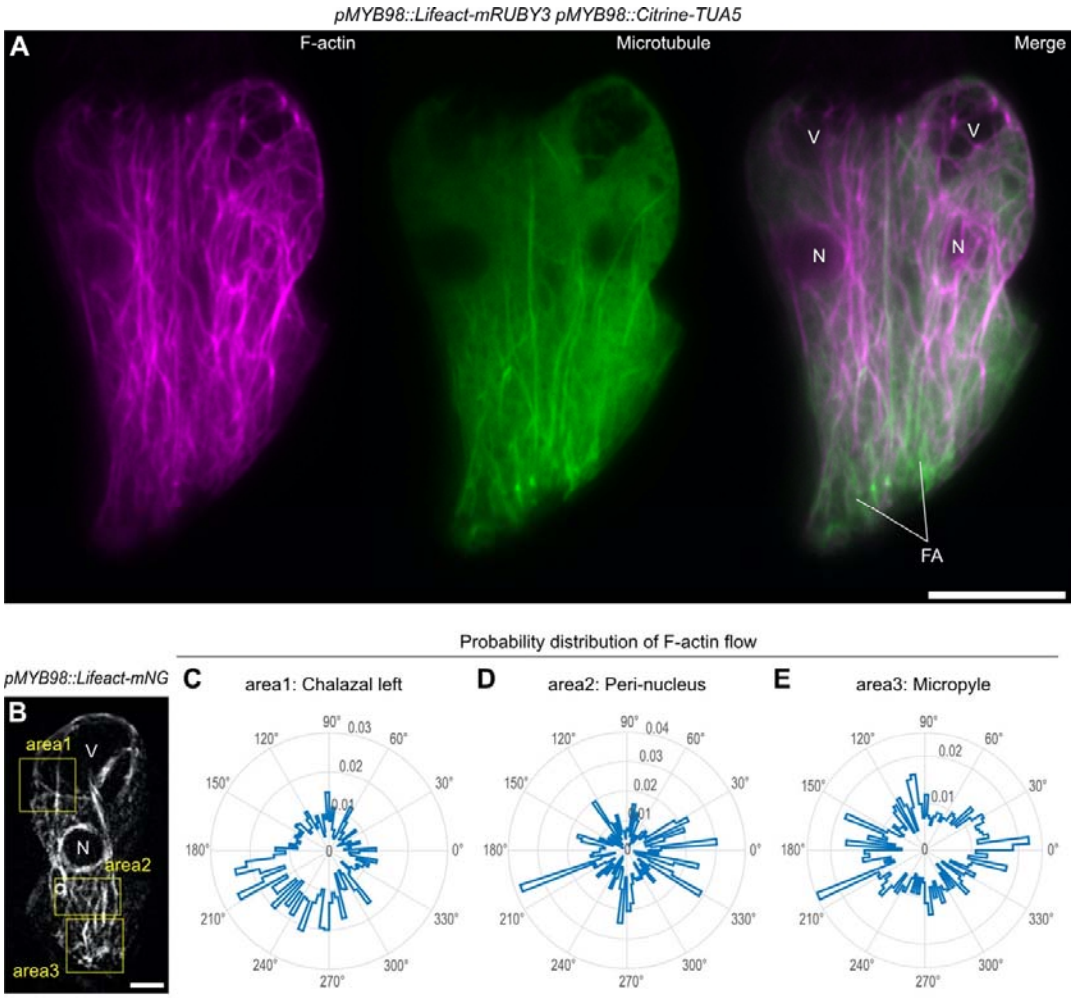

Figure 2 Distributions of cytoskeletons in synergid cells. **A,** Maximum intensity projection confocal images of a pair of synergid cells expressing *Lifeact-mRUBY3* F-actin marker (Magenta) and *Citrine-TUA5* microtubule marker (Green) from the *MYB98* promoter. **B,** The first frame of time-lapse imaging of F-actin dynamics in the synergid cell. A mature ovule in the transgenic plant expressing *Lifeact-mNeonGreen* F-actin marker (Grey) from the *MYB98* promoter (*pMYB98::Lifeact-mNG*) was captured in 30 sec intervals. The yellow boxes indicate the areas where F-actin flow was analyzed as shown in (C-E). V, vacuole; N, nucleus; FA, filiform apparatus; Scale bars, 10 µm in (A) and (B). **C-E,** Radar plots showing probability distributions of the directions of F-actin flow vectors in each area (the yellow box in (B)) obtained via spatiotemporal image correlation spectroscopy analysis. The probability was calculated from cumulative frequency of the F-actin flow vector angles obtained from the entire frames of time-lapse imaging. The probability values are scaled in the radial axes on the radar plots.

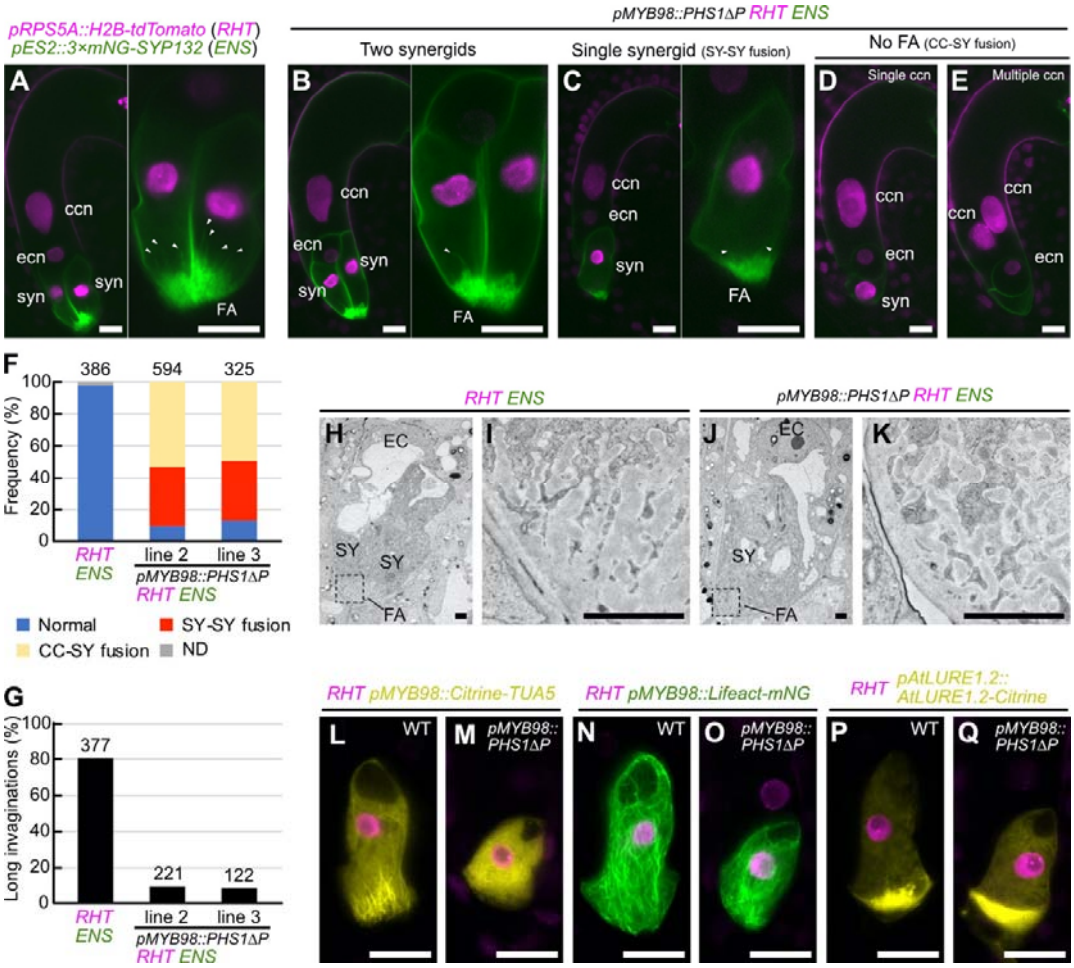

Figure 3 Microtubule is required for the growth of plasma membrane invaginations at the filiform apparatus. **A,** Wild-type ovule carrying the nuclear marker (*RHT*) and plasma membrane marker (*ENS*). **B–E,** Ovules containing two synergid cells (B), single synergid cell (C), a single central cell nucleus without filiform apparatus (D), or multiple central cell nuclei without filiform apparatus (E) observed in the *RHT;ENS* double marker line that were also homozygous for the microtubule destruction gene *PHS1ΔP* expressed from the *MYB98* promoter (*pMYB98::PHS1ΔP*). In (A–C), the synergid cell(s) in the left panel is magnified and shown in the right panel. **F, G,** Frequency of normal and aberrant female gametophyte (F) and percentages of filiform apparatus with long invaginations (G) in wild-type *RHT;ENS* line and two *pMYB98::PHS1ΔP;RHT;ENS* lines. **H–K,** Transmission electron micrographs of wild-type ovule in the *RHT;ENS* line (H) and single synergid cell-containing ovule of the *pMYB98::PHS1ΔP;RHT;ENS* line (J). Magnification of areas of the filiform apparatus indicated with dashed boxes in (H) and (J) were shown in (I) and (K), respectively. **L–Q,** Confocal images of synergid cells expressing *RHT* nuclear marker

1016 and other reporter genes showing synergid cell structures in wild-type plants (L, N, P)
1017 and *pMYB98::PHS1ΔP* transgenic lines (M, O, Q). The synergid cell-specific reporters
1018 were as follows: *pMYB98::Citrine-TUA5* (microtubules; L, M), *pMYB98::Lifeact-mNG*
1019 (F-actin; N, O), *pAtLURE1.2::AtLURE1.2-Citrine* (pollen tube attractant; P, Q).
1020 Abbreviations: *RHT*, *pRPS5A::H2B-tdTomato*; *ENS*, *pES2::3×mNG-SYP132*; ccn,
1021 central cell nucleus; ecn, egg cell nucleus; syn, synergid cell nucleus; FA, filiform
1022 apparatus; SY, synergid cell; EC, egg cell; CC, central cell. Scale bars: 20 μm in (A) to
1023 (E) and (L) to (Q); 2 μm in (H) to (K).
1024

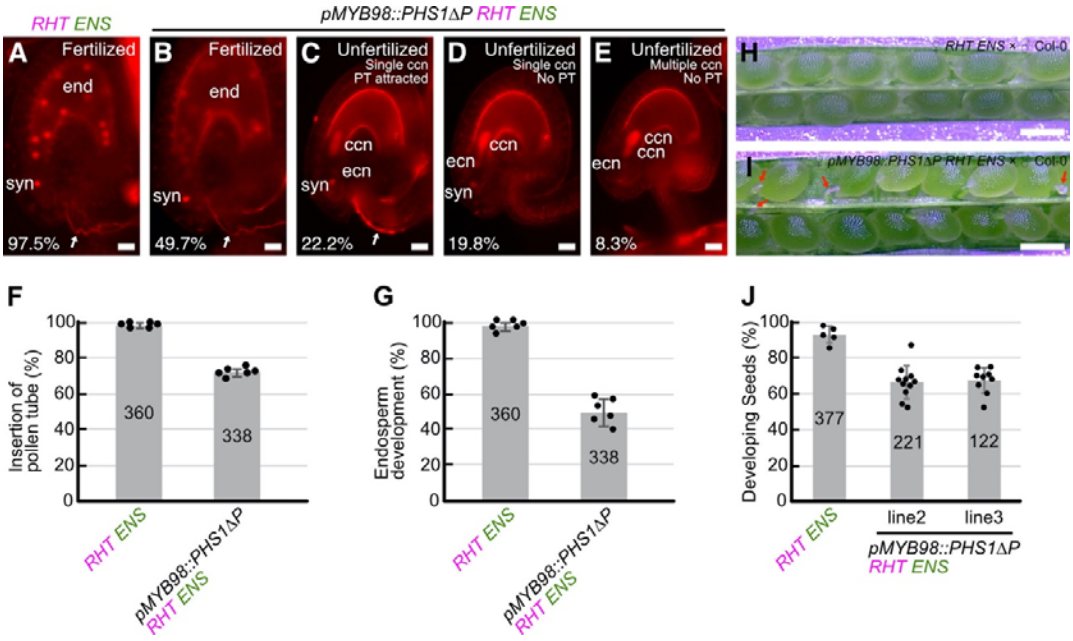

Figure 4 Fertilization of ovules expressing PHS1ΔP in synergid cells. **A–E,** Analysis of pollen tube attraction and seed development in wild-type plant carrying the nuclear marker (*RHT*) and plasma membrane marker (*ENS*) (A), and *pMYB98::PHS1ΔP;RHT;ENS* transgenic plant (B–E). Ovules were dissected from pistils at one day after pollination with wild-type Col-0 pollen and observed after CongoRed staining. Frequency of each ovule phenotype was shown in the bottom-left. White arrows indicate pollen tubes. **F, G,** Percentages of ovules displaying pollen tube insertions (F) and endosperm development (G). **H, I,** Representative images of developing seeds in pistils from wild-type *RHT;ENS* plant (H), and *pMYB98::PHS1ΔP;RHT;ENS* transgenic line (I), analyzed at eight days after pollination with wild-type Col-0 pollen. Red arrows indicate undeveloped ovules. **J,** Frequencies of developing seeds analyzed in (H) and (J). Abbreviations: *RHT*, *pRPS5A::H2B-tdTomato*; *ENS*, *pES2::3×mNG-SYP132*; ccn, central cell nucleus; ec n, egg cell nucleus; syn, synergid cell nucleus; end, endosperm nuclei. Scale bars: 20 μm in (A) to (E); 0.5 mm in (H) and (J).

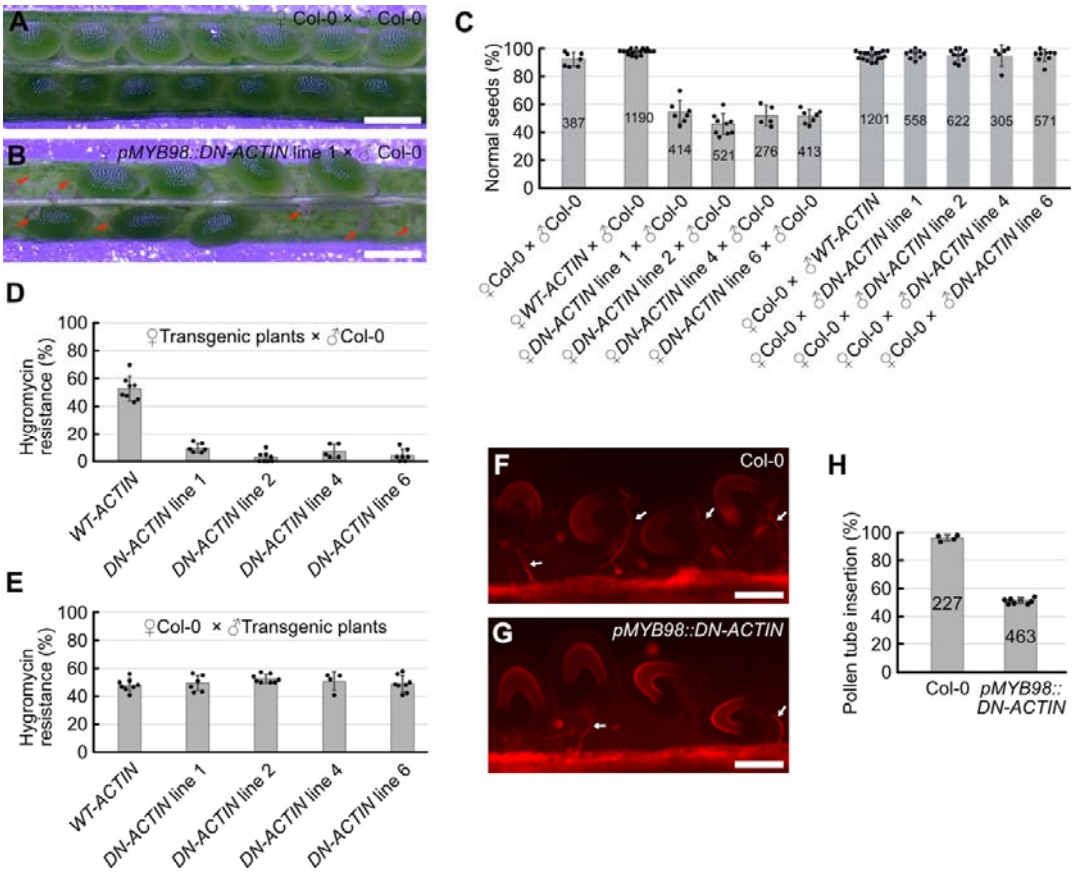

Figure 5 F-actin is required for pollen tube attraction. **A, B,** Representative images of developing seeds in pistils from wild-type Col-0 plants (A), and *pMYB98::DN-ACTIN* hemizygous lines (B), analyzed at eight days after pollination with wild-type Col-0 pollen. Red arrows indicate undeveloped ovules. **C,** Percentages of normal seeds harvested from pistils after various combinations of cross-pollination among wild-type Col-0 plants, *pMYB98::WT-ACTIN* hemizygous plants (*WT-ACTIN*), and *pMYB98::DN-ACTIN* hemizygous plants (*DN-ACTIN*). **D, E,** Transmissions of *pMYB98::WT-ACTIN* and *pMYB98::DN-ACTIN* transgenes via female gametophyte (D) or male gametophyte (E). Gene transmission was analyzed by frequencies of hygromycin-resistant F1 siblings generated by cross-pollinations in (B). **F, G,** Pollen tube growth pattern in pistils from wild-type Col-0 (F) and *pMYB98::DN-ACTIN* hemizygous (line 1) (G) plants. Pistils were pollinated with wild-type Col-0 pollen and the pollen tubes were visualized by a CongoRed staining at one day after pollination. White arrows indicate pollen tubes. **H,** Percentages of pollen tube-inserted ovules analyzed in (F) and (G). Scale bars: 0.5 mm in (A) and (B); 100 μm in (F) and (G).

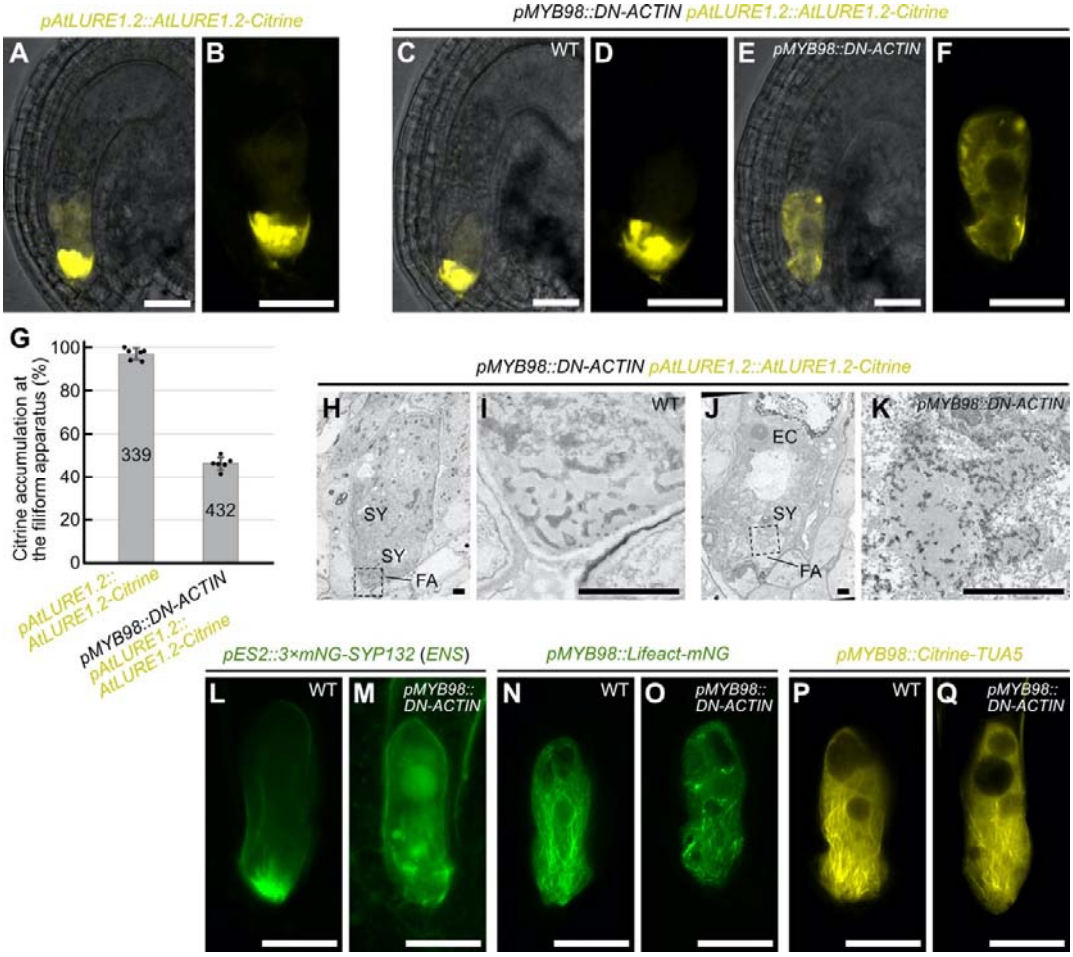

Figure 6 F-actin is necessary for directional protein secretion in synergid cell. **A–F,** Fluorescent signals of *pAtLURE1.2::AtLURE1.2-Citrine* pollen tube attractant marker in wild-type (A, B), and *pMYB98::DN-ACTIN* hemizygous (line 1) (C–F) plants. Merges of fluorescent images and differential interference contrast images were shown in (A), (C), and (E). Fluorescent images of magnified synergid cells were shown in (B), (D), and (F). The *pMYB98::DN-ACTIN* hemizygous plant showed segregation of wild-type ovules with normal fluorescent pattern (C, D), and abnormal ovules with little AtLURE1.2-Citrine signal at the filiform apparatus (E, F). **G,** Frequency of ovules displaying normal AtLURE1.2-Citrine accumulation at the filiform apparatus analyzed in (A) to (F). **H–K,** Transmission electron micrographs of wild-type (H, I) and abnormal (J, K) ovules segregated in pistils from a *pAtLURE1.2::AtLURE1.2-Citrine* transgenic plant hemizygous for the *pMYB98::DN-ACTIN* (line 1). Magnification of filiform apparatus indicated by dashed boxes in (H) and (J) were shown in (I) and (K), respectively. **L–Q,** Confocal images of synergid cells expressing plasma membrane marker (*pES2::3×mNG-SYP132*; L, M), F-actin marker (*pMYB98::Lifeact-mNG*; N, O),

1078 and microtubule marker (*pMYB98::Citrine-TUA5*; P, Q) in the *pMYB98::DN-ACTIN*
1079 hemizygous plants (line 1). Representative images of wild-type ovules (L, N, P) and
1080 aberrant ovules (M, O, Q) were shown. Abbreviations: FA, filiform apparatus; SY,
1081 synergid cell; EC, egg cell. Scale bars: 20 μm in (A) to (F) and (L) to (Q); 2 μm in (H)
1082 to (K).

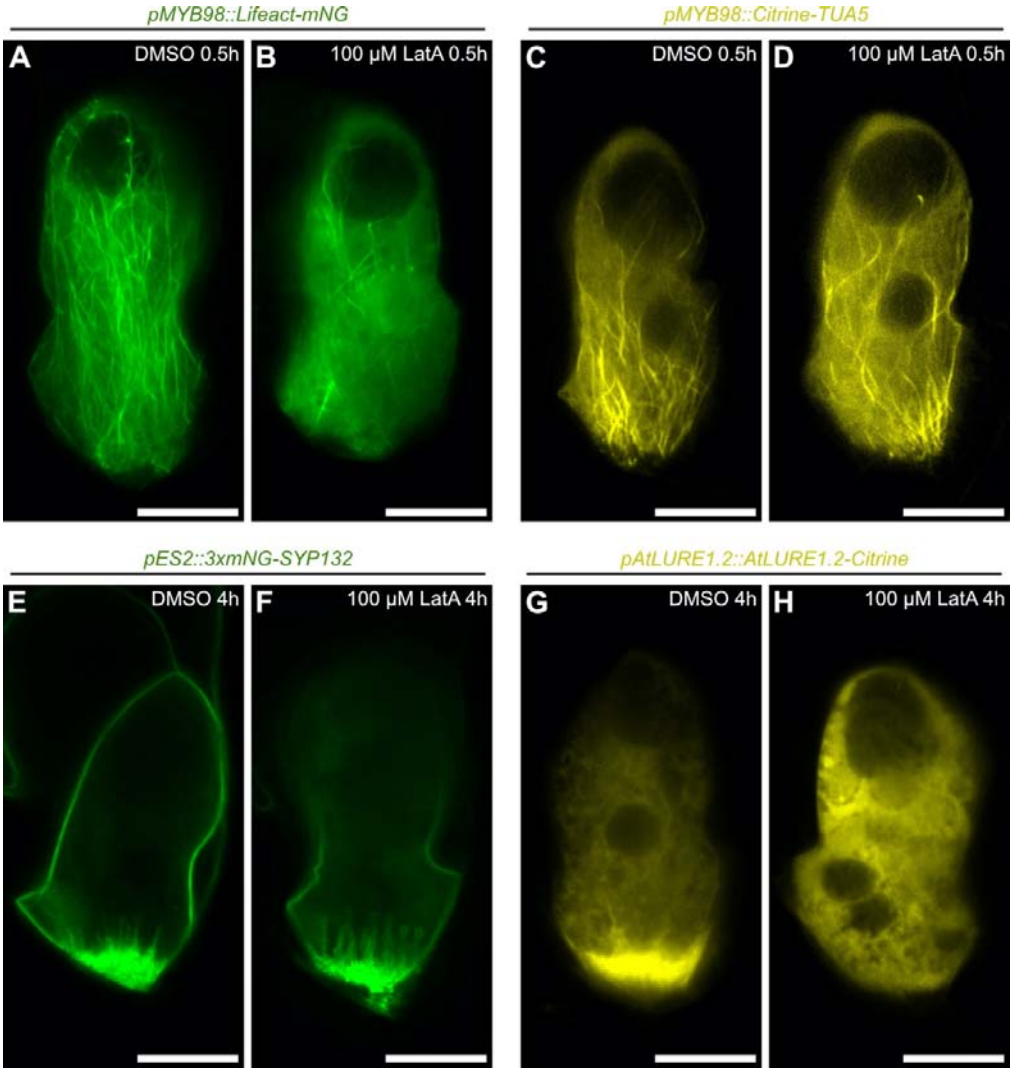

Figure 7 Transient actin depolymerization inhibits AtLURE1.2 accumulation without degeneration of the filiform apparatus. **A–H,** Confocal images of synergid cells in the *pMYB98::Lifeact-mNG* (F-actin marker line) (A, B), *pMYB98::Citrine-TUA5* (microtubule marker line) (C, D), *pES2::3×mNG-SYP132* (plasma membrane marker line) (E, F), and *pAtLURE1.2::AtLURE1.2-Citrine* (pollen tube attractant marker line) (G, H), cultured in a control medium containing 0.4% DMSO (A, C, E, G), or a medium containing 0.4% DMSO and 100 μM Latrunculin A (LatA) (B, D, F, H). Duration of the ovule culture is shown in the top-right. Scale bars: 20 μm.

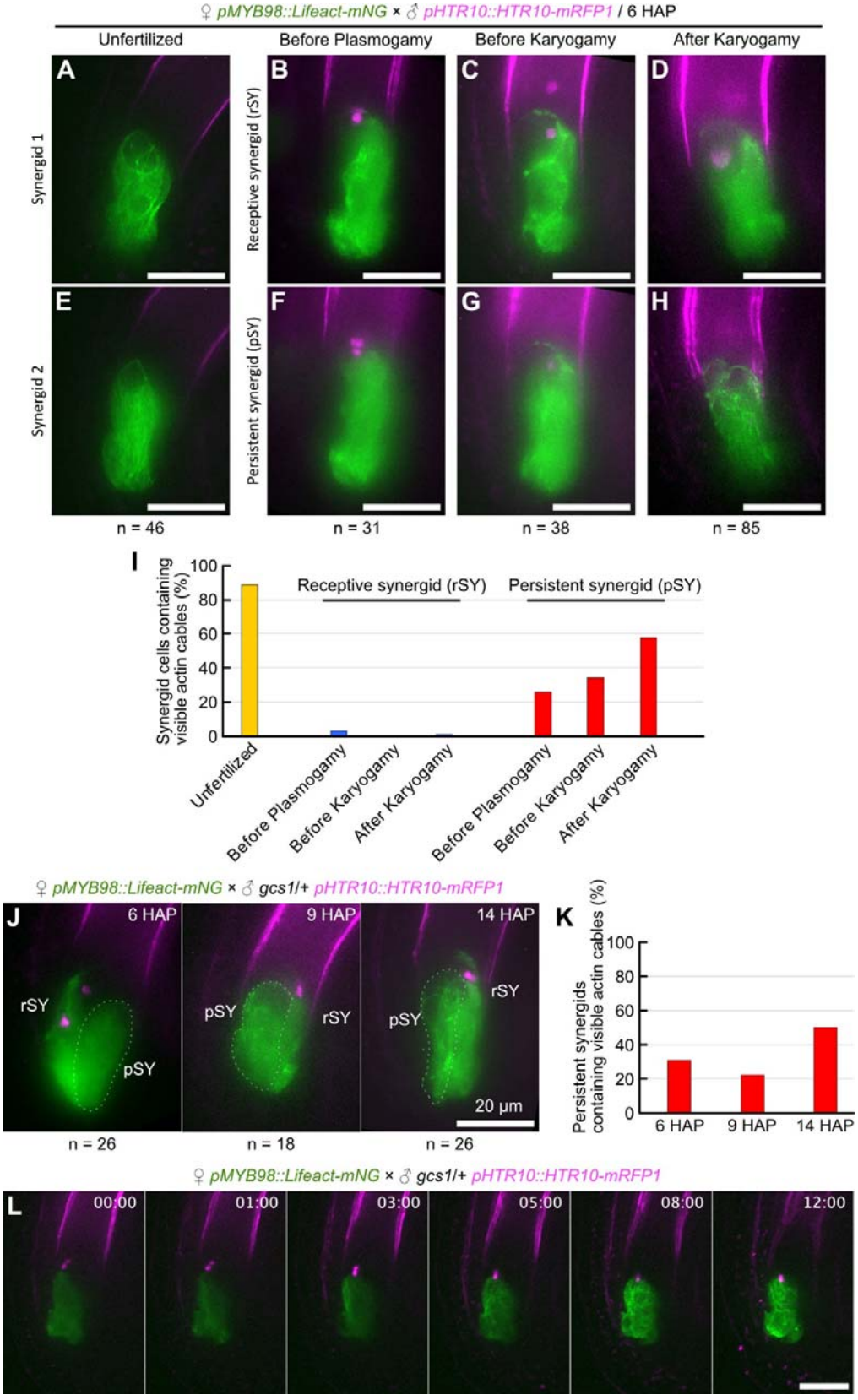
♀ pMYB98::Lifeact-mNG × ♂ pHTR10::HTR10-mRFP1 / 6 HAP
Unfertilized
Before Plasmogamy
Before Karyogamy
After Karyogamy
A
B
C
D
E
F
G
H
Synergid 1
Synergid 2
Receptive synergid (rSY)
Persistent synergid (pSY)
n = 46
n = 31
n = 38
n = 85
I
Synergid cells containing visible actin cables (%)
Receptive synergid (rSY)
Persistent synergid (pSY)
Unfertilized
Before Plasmogamy
Before Karyogamy
After Karyogamy
Before Plasmogamy
Before Karyogamy
After Karyogamy
♀ pMYB98::Lifeact-mNG × ♂ gcs1/+ pHTR10::HTR10-mRFP1
J
6 HAP
9 HAP
14 HAP
rSY
pSY
20 µm
n = 26
n = 18
n = 26
K
Persistent synergids containing visible actin cables (%)
6 HAP
9 HAP
14 HAP
♀ pMYB98::Lifeact-mNG × ♂ gcs1/+ pHTR10::HTR10-mRFP1
L
00:00
01:00
03:00
05:00
08:00
12:00

1093

1094 **Figure 8** Destruction and reconstruction of F-actin in the persistent synergid. **A–I,**
1095 F-actin pattern in the synergid cells during fertilization. Pistils from the
1096 *pMYB98::Lifeact-mNG* F-actin marker line were pollinated with pollen from the
1097 *pHTR10::HTR10-mRFP* sperm nuclear marker line and the ovules were analyzed at six
1098 hours after pollination (6 HAP) by spinning disk confocal microscopy. Images were
1099 maximum intensity projections of synergid cells on different focal planes in each
1100 Z-series of ovule at unfertilized stage (A, E), before plasmogamy stage (B, F), before
1101 karyogamy stage (C, G), and after karyogamy stage (D, H). After pollen tube reception,
1102 receptive synergids (rSY) (B, C, D) can be distinguished from persistent synergids
1103 (pSY) (E, F, H) by Lifeact-mNG leakage between the egg cell and central cell. The
1104 graph shows the percentage of synergid cells containing visible actin cables (I). **J–L,**
1105 F-actin pattern of the persistent synergids in the ovules after reception of
1106 fertilization-defective *gcs1* sperm cells. Pistils from the *pMYB98::Lifeact-mNG* were
1107 pollinated with pollen from a *gcs1* heterozygous plant carrying the
1108 *pHTR10::HTR10-mRFP* marker. Confocal images of ovules before plasmogamy at 6, 9,
1109 and 14 hours after pollination (J), and percentages of persistent synergids containing
1110 visible actin cables (K). Time-lapse imaging of an ovule dissected from a pistil at 6
1111 hours after pollination (L). Scale bars: 20 μm.

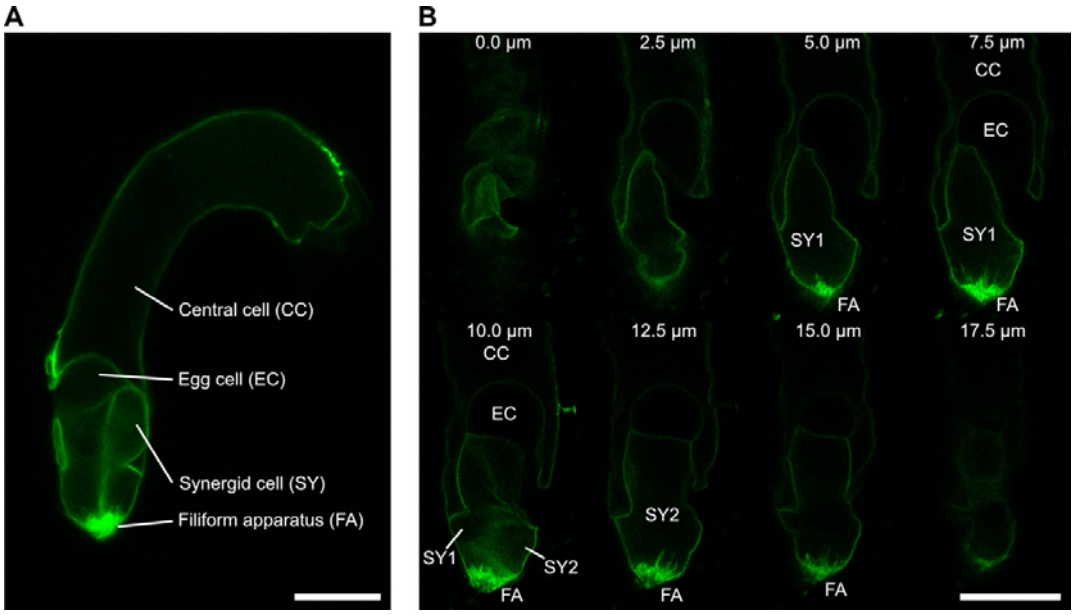

Figure S1 Confocal images of mature ovules from the *pES2::3×mNG-SYP132* (*ENS*) plasma membrane marker line. **A,** An image of center plane. **B,** Z-series images of a single ovule. Scale bars: 20 µm.

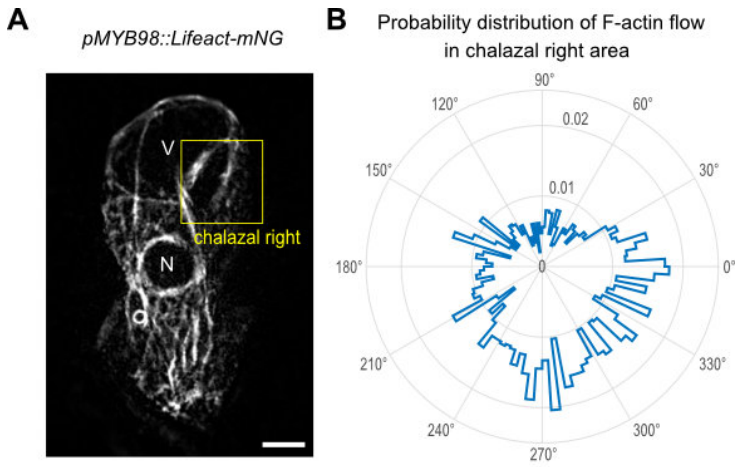

Figure S2 F-actin flow in the chalazal right area of synergid cell. **A,** The first frame of time-lapse imaging of F-actin (Grey) dynamics in the synergid cell expressing *pMYB98::Lifeact-mNG* (Figure 2B). The yellow box indicates the chalazal right area where F-actin flow was analyzed as shown in **B**. V, vacuole; N, nucleus; Scale bar, 10 µm. **B,** Radar plot displaying the probability distribution of F-actin flow directions in the chalazal right area (the yellow box in **A**). The directions are calculated from the angles of F-actin flow vectors obtained from spatiotemporal image correlation spectroscopy. The probability is calculated from cumulative frequency of the angles in F-actin flow vectors from the entire frames of time-lapse imaging and scaled in the radial axes on the radar plot.

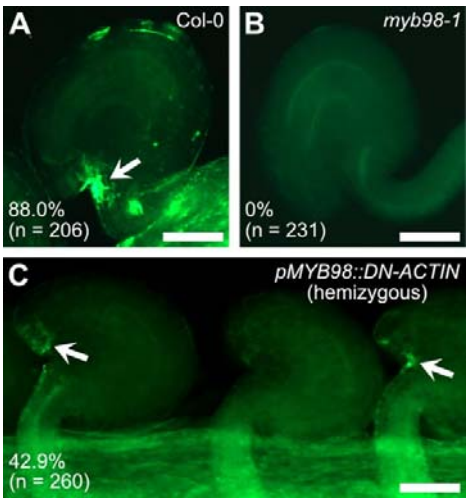

Figure S3 Immunostaining of AtLURE1.2. **A,** Wild-type ovule. **B,** *myb98-1* mutant ovule. **C,** Ovules in the *pMYB98::DN-ACTIN* hemizygous plant. Arrows represents AtLURE1.2 accumulation at the micropyle. Percentages of the AtLURE1.2 accumulation were shown in the bottom-left with the number of total ovules analyzed. Scale bars: 50 μm.

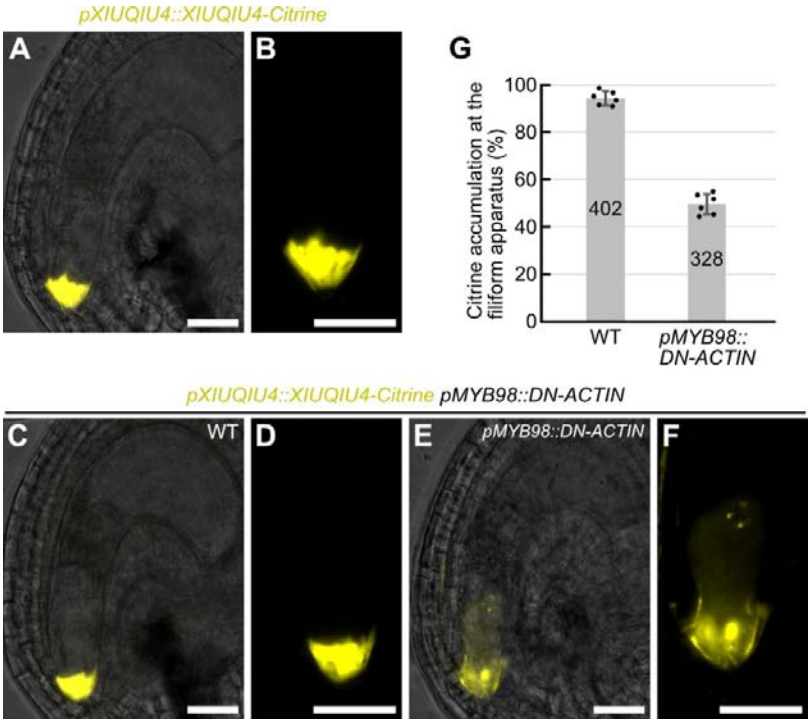

Figure S4 F-actin is necessary for directional XIUQIU4 secretion. **A–F,** Fluorescent signals of *pXIUQIU4::XIUQIU4-Citrine* pollen tube attractant marker in wild-type plant (A, B), and *pMYB98::DN-ACTIN* hemizygous plant (line 1) (C–F). Merges of fluorescent images and differential interference contrast images were shown in (A), (C), (E). Magnified synergid cells were shown in (B), (D), (F). The *pMYB98::DN-ACTIN* hemizygous plant showed segregation of wild-type ovules with normal fluorescent pattern (C, D), and abnormal ovules with little XIUQIU4-Citrine signal at the filiform apparatus (E, F). **G,** Frequency of ovules displaying normal XIUQIU4-Citrine accumulation at the filiform apparatus analyzed in (A) to (F). Scale bars: 20 μm.

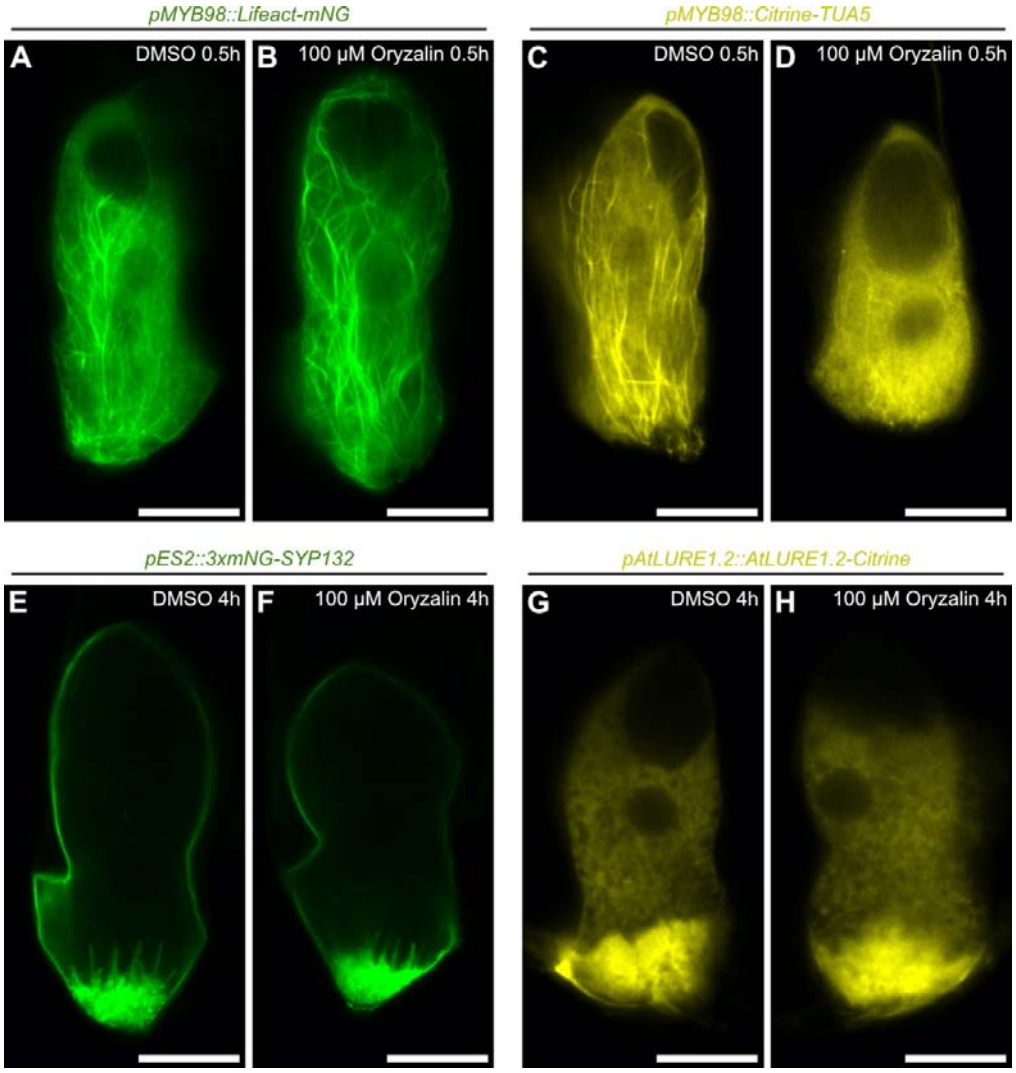

Figure S5 Transient microtubule depolymerization. **A–H,** Confocal images of synergid cells in the *pMYB98::Lifeact-mNG* (F-actin marker line) (A, B), *pMYB98::Citrine-TUA5* (Microtubule marker line) (C, D), *pES2::3×mNG-SYP132* (plasma membrane marker line) (E, F), and *pAtLURE1.2::AtLURE1.2-Citrine* (pollen tube attractant marker line) (G, H), cultured in a control medium containing 0.4% DMSO (A, C, E, G), or a medium containing 0.4% DMSO and 100 μM Oryzalin (B, D, F, H). Duration of the ovule culture is shown in the top-right. Scale bars: 20 μm.

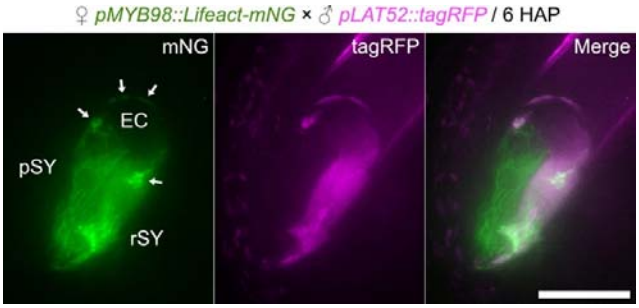

Figure S6 Moderate colocalization of actin corona-like structure and pollen tube cytosol.

Pistils from the *pMYB98::Lifeact-mNG* F-actin marker line were pollinated with pollen from the *pLAT52::tagRFP* pollen tube cytosolic marker line, and confocal images of an ovule were captured at six hour after pollination. Arrows represents the corona-like structures labeled with Lifeact-mNeonGreen. Abbreviations: EC, egg cell; rSY, receptive synergid; pSy, egg cell. Scale bar: 20 µm.

Table S1 Primers used in this study.

Primer name	Sequence (5' --> 3')
pENTR LifeActFP_F	CACCATGGGTGTCGCAGATTTGATCAAGAAATTCGAAAGCATCTCA AAGGAAGAAGGCGGCAGCGGCATGGTGAGCAAGGGCGAGGAG
FP_R	TTACTTGTACAGCTCGTCCATGCC
FP_SpeI_F	TGAACTAGTAAGGGTGGGCGCGC
FP_EcoRI_R	CATGAATTCGCTGCCGCCGCTG
SYP132_EcoRI_F	AGCGAATTCATGGACGATCTTCTGAAGGG
SYP132_SpeI_R	CTTACTAGTTCAAGCACTCTTGTTTTTC
GFP1-18_R	CTCGCCCTTGCTCACCAT
XFP_C-term_F	GGCATGGACGAGCTGTACAAG
GFP F	ATGGTGAGCAAGGGCGAGGA
Linker1_XFP_R	GGACAATGGTACCACATCCTTGTACAGCTCGTCCATGCC
Linker1_XFP_F	GATGTGGTACCATTGTCCATGGTGAGCAAGGGCGAGGA
Linker2_XFP_R	CACCAACAACATTTTGTGCTTGTACAGCTCGTCCATGCC
Linker2_XFP_F	CACAAAATGTTGTTGGTGATGGTGAGCAAGGGCGAGGA
Linker1_FP_F	GATGTGGTACCATTGTCCATGGTGAGCAAGGGCGAGGAA
pENTR_CFP_F	CACCATGGTGAGCAAGGGCGAGGAGC
pENTR_cacc_XFP_F	CCGCGGCCGCCCCCTTCACCATGGTGAGCAAGGGCGAGGA
FP_PstI_R	GACCTGCAGGCATGCAAGCTCTTGTACAGCTCGTCCAT
PHS1dP_F+SalI-TOPO	CACCGTCGACATGGTCACTAGTGCAGGAGAG
PHS1dP_R+AscI-stop	CTAGGCGCGCCCATTAGCAGCTTTGCTAATCA
AtLURE1.2_F+SalIGA	CTTGCATGCCTGCAGGTCGACGAGAGACATCAATGGATG
AtLURE1.2_-stopR+AscIGA	CTCCACCTCCAGAGGCGCGCCCTTTAATATCACTAATACTGCAAC
810_2.3_F+SalIGA	CTTGCATGCCTGCAGGTCGACGGATTGTTTGTTGGTCAG
810_2.3_-stopR+AscIGA	CTCCACCTCCAGAGGCGCGCCCCAAAATGTCTTCCAATGTA

1167

1168 ## Captions for Movies

1169

1170 **Movie 1** A 3D image of cell walls at the filiform apparatus reconstructed from serial
1171 sections obtained by FIB-SEM.

1172

1173 **Movie 2** A confocal z-series images of filiform apparatus in the
1174 *pMYB98::3×mNG-SYP132* plasma membrane marker line.

1175

1176 **Movie 3** Dynamics of F-actin in a synergid cell of mature ovule. Ovules from the
1177 *pMYB98::Lifeact-mNG* F-actin marker line were incubated in a liquid culture medium
1178 and subjected to time-lapse imaging using spinning disk confocal microscopy.

1179

1180 **Movie 4** F-actin dynamics of persistent synergids in two fertilized ovules. Pistils from
1181 the *pMYB98::Lifeact-mNG* were pollinated with pollen from a *gcs1* heterozygous plant
1182 carrying the *pHTR10::HTR10-mRFP* marker, and fertilized ovules displaying dispersed
1183 RFP signals of decondensed sperm-derived chromosomes in zygote nucleus and
1184 endosperm nucleus were analyzed by time-lapse imaging.

1185

1186 **Movie 5** F-actin dynamics of persistent synergids in three unfertilized ovules. Pistils
1187 from the *pMYB98::Lifeact-mNG* were pollinated with pollen from a *gcs1* heterozygous
1188 plant carrying the *pHTR10::HTR10-mRFP* marker, and unfertilized ovules containing a
1189 pair of punctate RFP signals of unfused sperm nuclei were analyzed by time-lapse
1190 imaging.

Parsed Citations

Ashdown, G., Pandžić, E., Cope, A., Wiseman, P., and Owen, D. (2015) Cortical Actin Flow in T Cells Quantified by Spatio-temporal Image Correlation Spectroscopy of Structured Illumination Microscopy Data. JoVE: 53749.
Google Scholar: Author Only Title Only Author and Title

Beale KM, Leydon AR, Johnson MA. (2012) Gamete fusion is required to block multiple pollen tubes from entering an Arabidopsis ovule. Curr Biol 22: 1090–1094
Google Scholar: Author Only Title Only Author and Title

Capron A, Gourgues M, Neiva LS, Faure JE, Berger F, Pagnussat G, Krishnan A, Alvarez-Mejia C, Vielle-Calzada JP, Lee YR, et al. (2008) Maternal control of male-gamete delivery in Arabidopsis involves a putative GPI-anchored protein encoded by the LORELEI gene. Plant Cell 20: 3038–3049
Google Scholar: Author Only Title Only Author and Title

Clough SJ, Bent AF. (1998) Floral dip: a simplified method for Agrobacterium-mediated transformation of Arabidopsis thaliana. Plant J 16: 735–743
Google Scholar: Author Only Title Only Author and Title

Diboll AG, Larson DA. (1966) An electron microscopic study of the mature megagametophyte in Zea mays. Am J Bot 53: 391–402
Google Scholar: Author Only Title Only Author and Title

Dresselhaus T, Sprunck S, Wessel GM. (2016) Fertilization Mechanisms in Flowering Plants. Curr Biol 26: R125–139
Google Scholar: Author Only Title Only Author and Title

Duan Q, Liu MJ, Kita D, Jordan SS, Yeh FJ, Yvon R, Carpenter H, Federico AN, Garcia-Valencia LE, Eyles SJ, et al., (2020) FERONIA controls pectin- and nitric oxide-mediated male-female interaction. Nature 579: 561–566
Google Scholar: Author Only Title Only Author and Title

Eng RC, Sampathkumar A. (2018) Getting into shape: the mechanics behind plant morphogenesis. Curr Opin Plant Biol 46: 25–31
Google Scholar: Author Only Title Only Author and Title

Escobar-Restrepo JM, Huck N, Kessler S, Gagliardini V, Gheyselinck J, Yang WC, Grossniklaus U. (2007) The FERONIA receptor-like kinase mediates male-female interactions during pollen tube reception. Science 317: 656–660
Google Scholar: Author Only Title Only Author and Title

Fujita S, Pytela J, Hotta T, Kato T, Hamada T, Akamatsu R, Ishida Y, Kutsuna N, Hasezawa S, Nomura Y et al. (2013) An atypical tubulin kinase mediates stress-induced microtubule depolymerization in Arabidopsis. Curr Biol 23: 1969–1978
Google Scholar: Author Only Title Only Author and Title

Galindo-Trigo S, Blanco-Tourinan N, DeFalco TA, Wells ES, Gray JE, Zipfel C, Smith LM. (2020) CrRLK1L receptor-like kinases HERK1 and ANJEA are female determinants of pollen tube reception. EMBO Rep 21: e48466
Google Scholar: Author Only Title Only Author and Title

Gooh K, Ueda M, Aruga K, Park J, Arata H, Higashiyama T, Kurihara D. (2015) Live-cell imaging and optical manipulation of Arabidopsis early embryogenesis. Dev Cell 34: 242–251
Google Scholar: Author Only Title Only Author and Title

Grossniklaus U. (2017) Polyspermy produces tri-parental seeds in maize. Curr Biol 27: R1300–R1302
Google Scholar: Author Only Title Only Author and Title

Hamamura Y, Saito C, Awai C, Kurihara D, Miyawaki A, Nakagawa T, Kanaoka MM, Sasaki N, Nakano A, Berger F. et al. (2011) Live-cell imaging reveals the dynamics of two sperm cells during double fertilization in Arabidopsis thaliana. Curr Biol 21: 497–502
Google Scholar: Author Only Title Only Author and Title

Heydlauff J, Serbes IE, Vo D, Mao Y, Gieseking S, Nakel T, Harten T, Völz R, Hoffmann A, Groß-Hardt R. (2022) Dual and opposing roles of EIN3 reveal a generation conflict during seed growth. Mol plant. 15: 363–371.
Google Scholar: Author Only Title Only Author and Title

Higashiyama T, Kuroiwa H, Kawano S, Kuroiwa T. (1998) Guidance in vitro of the pollen tube to the naked embryo sac of Torenia fournieri. Plant Cell 10: 2019–2031
Google Scholar: Author Only Title Only Author and Title

Huang B-Q, Russell SD. (1994) Fertilization in Nicotiana tabacum: cytoskeletal modifications in the embryo sac during synergid degeneration. Planta 194: 200–214
Google Scholar: Author Only Title Only Author and Title

Hwang D, Wada S, Takahashi A, Urawa H, Kamei Y, Nishikawa SI. (2019) Development of a Heat-Inducible Gene Expression System Using Female Gametophytes of Arabidopsis thaliana. Plant Cell Physiol 60: 2564–2572
Google Scholar: Author Only Title Only Author and Title

Ingouff M, Hamamura Y, Gourgues M, Higashiyama T, Berger F. (2007) Distinct dynamics of HISTONE3 variants between the two fertilization products in plants. Curr Biol 17: 1032–1037
Google Scholar: Author Only Title Only Author and Title

Iwano M, Ngo QA, Entani T, Shiba H, Nagai T, Miyawaki A, Isogai A, Grossniklaus U, Takayama S. (2012) Cytoplasmic Ca2+ changes dynamically during the interaction of the pollen tube with synergid cells. Development 139: 4202–4209
Google Scholar: Author Only Title Only Author and Title

Jensen WA. (1965) The ultrastructure and histochemistry of the synergids of cotton. Am J Bot 52: 238–256
Google Scholar: Author Only Title Only Author and Title

Johnson MA, Harper JF, Palanivelu R. (2019) A Fruitful Journey: Pollen Tube Navigation from Germination to Fertilization. Annu Rev Plant Biol 70: 809–837
Google Scholar: Author Only Title Only Author and Title

Ju Y, Yuan J, Jones DS, Zhang W, Staiger CJ, Kessler SA. (2021) Polarized NORTIA accumulation in response to pollen tube arrival at synergids promotes fertilization. Dev Cell 56: 2938–2951 e6
Google Scholar: Author Only Title Only Author and Title

Kawashima T, Maruyama D, Shagirov M, Li J, Hamamura Y, Yelagandula R, Toyama Y, Berger F. (2014) Dynamic F-actin movement is essential for fertilization in Arabidopsis thaliana. Elife 3: e04501
Google Scholar: Author Only Title Only Author and Title

Kasahara RD, Portereiko MF, Sandaklie-Nikolova L, Rabiger DS, Drews GN. (2005) MYB98 is required for pollen tube guidance and synergid cell differentiation in Arabidopsis. Plant Cell 17: 2981–2992.
Google Scholar: Author Only Title Only Author and Title

Kasahara RD, Maruyama D, Hamamura Y, Sakakibara T, Twell, D, Higashiyama, T. (2012) Fertilization recovery after defective sperm cell release in Arabidopsis. Curr. Biol. 22: 1084–1089.
Google Scholar: Author Only Title Only Author and Title

Kato T, Morita MT, Tasaka M. (2010) Defects in dynamics and functions of actin filament in Arabidopsis caused by the dominant-negative actin fiz1-induced fragmentation of actin filament. Plant Cell Physiol 51: 333–338
Google Scholar: Author Only Title Only Author and Title

Kessler SA, Shimosato-Asano H, Keinath NF, Wuest SE, Ingram G, Panstruga R, Grossniklaus U. (2010) Conserved molecular components for pollen tube reception and fungal invasion. Science 330: 968–971
Google Scholar: Author Only Title Only Author and Title

Li C, Yeh FL, Cheung AY, Duan Q, Kita D, Liu MC, Maman J, Luu EJ, Wu BW, Gates L et al. (2015) Glycosylphosphatidylinositol-anchored proteins as chaperones and co-receptors for FERONIA receptor kinase signaling in Arabidopsis. Elife 4: e06587
Google Scholar: Author Only Title Only Author and Title

Li W, Li Q, Lyu M, Wang Z, Song Z, Zhong S, Gu H, Dong J, Dresselhaus T, Zhong S et al. (2022) Lack of ethylene does not affect reproductive success and synergid cell death in Arabidopsis. Mol Plant 15: 354–362
Google Scholar: Author Only Title Only Author and Title

Mansfield SG, Briarty LG, Erni S. (1991) Early embryogenesis in Arabidopsis thaliana. I. The mature embryo sac. Can J Bot 69: 447–460
Google Scholar: Author Only Title Only Author and Title

Mao Y, Gabel A, Nakel T, Viehöver P, Baum T, Tekleyohans DG, Vo D, Grosse I, Groß-Hardt R. (2020) Selective egg cell polyspermy bypasses the triploid block. Elife 9: e52976
Google Scholar: Author Only Title Only Author and Title

Marton ML, Cordts S, Broadhvest J, Dresselhaus T. (2005) Micropylar pollen tube guidance by egg apparatus 1 of maize. Science 307: 573–576
Google Scholar: Author Only Title Only Author and Title

Marton ML, Fastner A, Uebler S, Dresselhaus T. (2012) Overcoming hybridization barriers by the secretion of the maize pollen tube attractant ZmEA1 from Arabidopsis ovules. Curr Biol 22: 1194–1198
Google Scholar: Author Only Title Only Author and Title

Maruyama D, Hamamura Y, Takeuchi H, Susaki D, Nishimaki M, Kurihara D, Kasahara RD, Higashiyama T. (2013) Independent control by each female gamete prevents the attraction of multiple pollen tubes. Dev Cell 25: 317–323
Google Scholar: Author Only Title Only Author and Title

Maruyama D, Völz R, Takeuchi H, Mori T, Igawa T, Kurihara D, Kawashima T, Ueda M, Ito M, Umeda M et al. (2015) Rapid Elimination of the Persistent Synergid through a Cell Fusion Mechanism. Cell 161: 907–918
Google Scholar: Author Only Title Only Author and Title

Maruyama D, Higashiyama T. (2016) The end of temptation: the elimination of persistent synergid cell identity. Curr Opin in Plant Biol 34: 122–126
Google Scholar: Author Only Title Only Author and Title

Meng J-G, Zhang M-X, Yang, W-C, Li H-J. (2019) TICKET attracts pollen tubes and mediates reproductive isolation between relative species in Brassicaceae. Sci China Life Sci 62: 1413–1419
Google Scholar: Author Only Title Only Author and Title

Mori T, Kuroiwa H, Higashiyama T, Kuroiwa T. (2006) GENERATIVE CELL SPECIFIC 1 is essential for angiosperm fertilization. Nat Cell Biol 8: 64–71
Google Scholar: Author Only Title Only Author and Title

Nakagawa T, Suzuki T, Murata S, Nakamura S, Hino T, Maeo K, Tabata R, Kawai T, Tanaka K, Niwa Y et al. (2007) Improved Gateway binary vectors: high-performance vectors for creation of fusion constructs in transgenic analysis of plants. Biosci Biotechnol Biochem 71: 2095–2100
Google Scholar: Author Only Title Only Author and Title

Nakel T, Tekleyohans DG, Mao Y, Fuchert G, Vo D, Groß-Hardt R. (2017) Triparental plants provide direct evidence for polyspermy induced polyploidy. Nat commun. 8: 1–8
Google Scholar: Author Only Title Only Author and Title

Ngo QA, Vogler H, Lituiev DS, Nestorova A, Grossniklaus U. (2014) A calcium dialog mediated by the FERONIA signal transduction pathway controls plant sperm delivery. Dev Cell 29: 491–500
Google Scholar: Author Only Title Only Author and Title

Ohnishi Y, Hoshino R, Okamoto T. (2014) Dynamics of Male and Female Chromatin during Karyogamy in Rice Zygotes Plant Physiol 165: 1533–1543
Google Scholar: Author Only Title Only Author and Title

Ohnishi Y, Okamoto T. (2015) Karyogamy in rice zygotes: Actin filament-dependent migration of sperm nucleus, chromatin dynamics, and de novo gene expression

Plant Signal & Behav 10: e989021

Oi T, Enomoto S, Nakao T, Arai S, Yamane K, Taniguchi M. (2017) Three-dimensional intracellular structure of a whole rice mesophyll cell observed with FIB-SEM. Ann Bot 120: 21–28
Google Scholar: Author Only Title Only Author and Title

Okuda S, Tsutsui H, Shiina K, Sprunck S, Takeuchi H, Yui R, Kasahara RD, Hamamura Y, Mizukami A, Susaki D, et al. (2009) Defensin-like polypeptide LUREs are pollen tube attractants secreted from synergid cells. Nature 458: 357–361
Google Scholar: Author Only Title Only Author and Title

Pagnussat GC, Yu HJ, Sundaresan V. (2007) Cell-fate switch of synergid to egg cell in Arabidopsis eostre mutant embryo sacs arises from misexpression of the BEL1-like homeodomain gene BLH1. Plant Cell 19: 3578–3592
Google Scholar: Author Only Title Only Author and Title

Pereira AM, Nobre MS, Pinto SC, Lopes AL, Costa ML, Masiero S, Coimbra S. (2016) "Love Is Strong, and You're so Sweet": JAGGER Is Essential for Persistent Synergid Degeneration and Polytubey Block in Arabidopsis thaliana. Mol Plant 9: 601–614
Google Scholar: Author Only Title Only Author and Title

Leshem Y, Johnson C, Sundaresan V. (2013) Pollen tube entry into the synergid cell of Arabidopsis is observed at a site distinct from the filiform apparatus. Plant reproduction 26: 93–99.
Google Scholar: Author Only Title Only Author and Title

Riedl J, Crevenna AH, Kessenbrock K, Yu JH, Neukirchen D, Bista M, Bradke F, Jenne D, Holak TA, Werb Z et al. (2008) Lifeact: a versatile marker to visualize F-actin. Nat. Methods 5: 605–607.
Google Scholar: Author Only Title Only Author and Title

Russell SD. (1993) The egg cell: development and role in fertilization and early embryogenesis. Plant Cell 5: 1349–1359
Google Scholar: Author Only Title Only Author and Title

Schindelin J, Arganda-Carreras I, Frise E, Kaynig V, Longair M, Pietzsch T, Preibisch S, Rueden C, Saalfeld S, Schmid B et al. (2012) Fiji: an open-source platform for biological-image analysis. Nature methods 9: 676-82.
Google Scholar: Author Only Title Only Author and Title

Schulz R, Jensen, WA. (1968) Capsella embryogenesis: the synergids before and after fertilization. Am J Bot 55: 541–552
Google Scholar: Author Only Title Only Author and Title

Shaner NC, Lambert GG, Chammas A, Ni Y, Cranfill PJ, Baird MA, Sell BR, Allen JR, Day RN, Israelsson M et al. (2013) A bright monomeric green fluorescent protein derived from Branchiostoma lanceolatum. Nat. Methods 10: 407–409
Google Scholar: Author Only Title Only Author and Title

Stephan OOH. (2017) Actin fringes of polar cell growth. J Exp Bot 68: 3303–3320
Google Scholar: Author Only Title Only Author and Title

Susaki D, Suzuki T, Maruyama D, Ueda M, Higashiyama T, Kurihara D. (2021) Dynamics of the cell fate specifications during female gametophyte development in Arabidopsis. PLoS Biol 19: e3001123
Google Scholar: Author Only Title Only Author and Title

Takeuchi H, Higashiyama T. (2012) A species-specific cluster of defensin-like genes encodes diffusible pollen tube attractants in Arabidopsis. PLoS Biol 10: e1001449
Google Scholar: Author Only Title Only Author and Title

Takeuchi H, Higashiyama T. (2016) Tip-localized receptors control pollen tube growth and LURE sensing in Arabidopsis. Nature 531: 245–248
Google Scholar: Author Only Title Only Author and Title

Tsukamoto T, Qin Y, Huang Y, Dunatunga D, Palanivelu R. (2010) A role for LORELEI, a putative glycosylphosphatidylinositol-anchored protein, in Arabidopsis thaliana double fertilization and early seed development. Plant J 62: 571–588
Google Scholar: Author Only Title Only Author and Title

Uemura T, Ueda T, Ohniwa RL, Nakano A, Takeyasu K, Sato MH. (2004) Systematic analysis of SNARE molecules in Arabidopsis: dissection of the post-Golgi network in plant cells. Cell Struc. Funct. 29: 49–65.
Google Scholar: Author Only Title Only Author and Title

Völz R, Heydlauff J, Ripper D, von Lyncker L, Groß-Hardt R. (2013) Ethylene signaling is required for synergid degeneration and the establishment of a pollen tube block. Dev Cell 25: 310–316
Google Scholar: Author Only Title Only Author and Title

von Besser K, Frank AC, Johnson MA, Preuss D. (2006) Arabidopsis HAP2 (GCS1) is a sperm-specific gene required for pollen tube guidance and fertilization Development 133: 4761–4769
Google Scholar: Author Only Title Only Author and Title

Webb MC, Gunning BES. (1994) Embryo sac development in Arabidopsis thaliana II. The cytoskeleton during megagametogenesis. Sex. Plant Reprod. 7: 153–163
Google Scholar: Author Only Title Only Author and Title

Yu HJ, Hogan P, Sundaresan V. Analysis of the female gametophyte transcriptome of Arabidopsis by comparative expression profiling. Plant physiology. (2005) 139: 1853–1869.
Google Scholar: Author Only Title Only Author and Title

Yu X, Zhang X, Zhao P, Peng X, Chen H, Bleckmann A, Bazhenova A, Shi C, Dresselhaus T, Sun MX. (2021) Fertilized egg cells secrete endopeptidases to avoid polytubey. Nature 592: 433–437
Google Scholar: Author Only Title Only Author and Title

Zhong S, Liu M, Wang Z, Huang Q, Hou S, Xu YC, Ge Z, Song Z, Huang J, Qiu X et al. (2019) Cysteine-rich peptides promote interspecific genetic isolation in Arabidopsis. Science 364: eaau9564
Google Scholar: Author Only Title Only Author and Title

Zhong S, Li L, Wang Z, Ge Z, Li Q, Bleckmann A, Wang J, Song Z, Shi Y, Liu T et al. (2022) RALF peptide signaling controls the polytubey block in Arabidopsis. Science 375: 290-296.
Google Scholar: Author Only Title Only Author and Title